Calculation of the hyperfine interaction using an effective-operator form of many-body theory

Sten Garpman, Ingvar Lindgren, Johannes Lindgren, and John Morrison
Chalmers University of Technology and the University of Göteborg, Göteborg, Sweden
(Received 15 July 1974)

The effective-operator form of many-body theory is reviewed and applied to the calculation of the hyperfine structure. Numerical results are given for the $2p$, $3p$, and $4p$ excited states of Li and the $3p$ state of Na. This is the first complete calculation of the hyperfine structure using an effective-operator form of perturbation theory. As in the Brueckner-Goldstone form of many-body theory, the various terms in the perturbation expansion are represented by Feynman diagrams which correspond to basic physical processes. The angular part of the perturbation diagrams are evaluated by taking advantage of the formal analogy between the Feynman diagrams and the angular-momentum diagrams, introduced by Jucys *et al.* The radial part of the diagrams is calculated by solving one- and two-particle equations for the particular linear combination of excited states that contribute to the Feynman diagrams. In this way all second- and third-order effects are accurately evaluated without explicitly constructing the excited orbitals. For the $2p$ state of Li our results are in agreement with the calculations of Nesbet and of Hameed and Foley. However, our quadrupole calculation disagrees with the work of Das and co-workers. The many-body results for Li and Na are compared with semiempirical methods for evaluating the quadrupole moment from the hyperfine interaction and a new quadrupole moment of ^{23}Na is given.

I. INTRODUCTION

In recent years a large number of calculations of the atomic hyperfine structure have been reported. The calculations which are the most accurate and which have the widest area of application employ the linked-diagram perturbative formalism or some kind of variational technique. Each of these approaches takes into account configuration mixing in a systematic way; however, they require an extensive effort for each atomic state, and the success of the calculation depends inevitably upon technical details which an ordinary reader could not be expected to evaluate.

The linked-diagram perturbation formalism was developed by Brueckner[1] and Goldstone,[2] and first applied to atomic problems by Kelly.[3] In perturbative calculations of this kind, the atomic Hamiltonian (H) is decomposed into a single-particle operator (H_0) and a term which corresponds to the residual part of the Coulomb interaction among the electrons (V). In a hyperfine problem there is an additional operator which describes the interaction of the electrons with the hyperfine field of the nucleus. This last operator can be written

$$h = \sum_i \left[a_l r_i^{-3} \vec{l}_i + a_{sd} r_i^{-3} (\vec{s}_i \cdot \vec{C}_i^{(2)})^{(1)} + a_s \delta(\vec{r}_i)\vec{s}_i\right] \cdot \vec{\mu} + \sum_i a_q r_i^{-3} \vec{C}^{(2)} \circ \vec{Q} , \quad (1)$$

where $\vec{s}$, $\vec{l}$, and $\vec{C}^{(2)}$ are the single-electron spin, orbital, and quadrupole operators; a_l, a_{sd}, a_s, and a_q are physical constants; and $\vec{\mu}$ and $\vec{Q}$ are the magnetic dipole moment and the electric quadrupole moment of the nucleus, respectively. In order to perform the calculation, a complete set of solutions of the single-particle Hamiltonian is obtained, and the zeroth-order wave function is normally expressed as a single determinant of these solutions. Corrections to the wave function and the energy due to the other parts of H may then be expressed in terms of diagrams. The most difficult part of these calculations consists in selecting all of the important diagrams and in carrying out summations and integrations over the excited states. The excited functions often have different spatial properties than the occupied orbitals. Also it should be noted that the scope of such "single-determinantal" calculations is necessarily quite limited. While the (Hund's-rule) ground state of an atom may often be represented by a single determinant, the metastable states usually have quite complicated expansions in terms of determinants, even though they have a well-defined angular symmetry. Recently, a good deal of emphasis has been placed upon experimental methods of populating metastable states, and it is therefore of great interest to be able to perform calculations on *all* states within a configuration.

In the variational calculations, such as those performed by Nesbet,[4] the wave function is constructed out of a finite basis set, and the total energy is minimized within this set. For this purpose, basis functions having well-defined values of L and S may be employed. A symmetry adopted approach of this kind has been used ex-

tensively by Weiss,[5] and Hameed and Foley[6] have used his wave functions to calculate the hyperfine structure of Li $2p$. The metastable states offer no special difficulties for such an approach; however, a separate calculation must be performed for each atomic state, and a set of basis functions must be used which includes all of the significant effects. The choice of a basis set is the most difficult part of such calculations.

In this paper we apply an effective-operator form of many-body theory to calculate the atomic hyperfine structure. The basic idea of an effective-operator approach is to describe the interactions of the electrons by an effective interaction operator, which acts within a certain subspace (model space), normally a single configuration. The effect of configuration mixing is thus to modify the form of the interaction rather than to change the wave functions. There is already a good deal of experimental justification for such an approach. Harvey[7] has shown that the magnetic hyperfine interaction of oxygen and fluorine could be successfully described by allowing the $\langle r^{-3}\rangle$ values associated with a_s, a_l, and a_{sd} in Eq. (1) to have independent values. This kind of parametric treatment has been used extensively in analyzing experimental hyperfine data.[8]

The mathematical formulation of the effective-operator approach is due to a number of authors. Early work related to nuclear problems was done in this field by Eden and Francis[9], Feshbach,[10] and Bloch and Horowitz.[11] This formalism, however, is based on the Brillouin-Wigner type of perturbation and, therefore, leads to energy-dependent effective operators, so the calculations have to be performed for one state at a time. It was later shown by Brandow[12] that the energy dependence can be eliminated by expanding the energy shift out of the denominators. This expansion essentially cancels so-called unlinked diagrams, so that only linked diagrams remain.

An effective-operator formalism which is suitable for atomic calculations was developed by Judd,[13] Wybourne,[14] and others, following early ideas of Trees[15] and Racah.[16] The mathematical formulation of this approach is based on an article of Bloch[17] on the effect of a perturbation upon a degenerate space. In his treatment, Bloch employed the Rayleigh-Schrödinger (RS) form of perturbation theory, which leads directly to an energy-independent expansion of the effective operator. A simple proof of the linked-diagram theorem, based on this formalism, has been given by Sandars[18] for a model space with a single configuration, and this treatment has recently been extended by one of us (IL) to the multiconfigurational case.[19] Most of the works mentioned above employ a time-independent technique, but essentially equivalent results can be obtained by time-dependent methods, as shown by several authors.[20]

There are thus three interrelated lines of development of the effective-operator form of perturbation theory. Each of these leads to a linked-diagram (LD) theorem and to certain diagrams peculiar to the degenerate case, for which open-shell lines are directed downward. Brandow called these additional diagrams, which are necessary to cancel the unlinked diagrams, "folded" diagrams. In the time-dependent form of perturbation theory a line directed downward may be interpreted as a particle moving backward in time, and so these diagrams have also been referred to as "backward" diagrams.[18]

The perturbation expansion is conveniently represented by means of Feynman diagrams.[1-3] In problems based on the central-field model there is a close analogy between the Feynman diagrams and the angular-momentum diagrams, introduced by Yutsis *et al.*[21] This enables one to evaluate the angular part of the perturbation diagrams in atomic calculations in a very elegant way.[13,18] The radial part of the diagrams may either be calculated by solving for a complete set of states and calculating the effect of each excitation separately, or by setting up one- and two-particle equations for the particular linear combination of excited states that contribute to the Feynman diagrams. A single-particle function that satisfies a first-order equation of this kind has been used extensively by Sternheimer[22] to calculate the perturbing effect of the quadrupole moment of a nucleus upon the core electrons, and recently accurate finite-difference methods have become available for solving such two-particle equations.[23]

While there is an extensive literature of effective-operator calculations in nuclear theory,[20] very few applications have been reported of these techniques to an atomic system. Morrison and Rajnak[24] have used this approach to calculate the effective interaction of the two $4f$ electrons of Pr^{3+}. In their calculation, they used the numerical techniques developed by Kelly[3] and applied extensively by Das and his co-workers,[25] which entail solving for a complete set of excited states. The Pr^{3+} calculation was then repeated, however, by solving inhomogeneous one- and two-particle equations for the particular linear combination of excited states, which contribute to the second- and third-order diagrams.[26] This technique, which is described in Sec. V, together with the effective-operator form of perturbation theory represents a very powerful and general theoretical tool. It enables one to calculate the effect of a perturbation

upon all of the states of an atomic configuration, and it yields second- and third-order values accurate to four significant figures, which is the accuracy of the solution of the associated differential equations. We are thus in a position to extend the realm of theoretical work and to check the accuracy of previous many-body calculations.

In this paper we summarize the theoretical methods and then report the results of calculations of the hyperfine structure of the $2p$, $3p$, and $4p$ excited states of Li and the $3p$ state of Na. The hyperfine structure of Li $2p$ has previously been calculated by Nesbet[4] using variational methods, by Lyons, Pu, and Das[25] using Brueckner-Goldstone perturbation theory, and by Hameed and Foley.[6] Our results are in good agreement with those of Nesbet for both the magnetic dipole and electric quadrupole interaction constants. Also our quadrupole calculation agrees fairly well with that of Hameed and Foley. For the orbital and spin-dipole cases, there is a general agreement between our values of the Feynman diagrams and those calculated by Das and co-workers. However, there are numerous discrepancies between their calculation and ours for the quadrupole case. The many-body results for Li and Na are compared with various semiempirical methods for evaluating the quadrupole moment from the hyperfine interaction and a new quadrupole moment of ^{23}Na is given.

II. PERTURBATION THEORY AND EFFECTIVE OPERATORS

The aim of perturbation theory is to yield an approximate solution of the Schrödinger equation,

$$H\Psi^\alpha = E^\alpha \Psi^\alpha , \tag{2}$$

of a physical system with an arbitrary degree of accuracy. For this purpose, the Hamiltonian is split into two parts, an approximate or model Hamiltonian H_0 and a perturbation V:

$$H = H_0 + V . \tag{3}$$

For atomic systems it is usually convenient to choose H_0 to be a central-field Hamiltonian of the form

$$H_0 = \sum_i \left(-\frac{1}{2}\nabla_i^2 - \frac{Z}{r_i} + U(r_i) \right) = \sum_i h^0(i) , \tag{4}$$

which describes a system of electrons moving in some average central field due to the nucleus and the other electrons. The single-particle states may then be written as

$$\Psi(nl m_s m_l) = r^{-1} P_{nl}(r) Y^l_{m_l}(\theta, \phi) \chi_{m_s}(\sigma) , \tag{5}$$

and the eigenstates of H_0 may be chosen to be Slater determinants, for which a certain number of these single-particle states are occupied. The perturbation is then the noncentral part of the Coulomb interaction among the electrons, and it may also include the interaction of the electrons with an external field, such as the hyperfine field of the nucleus

$$V = \left(\sum_{i>j} \frac{1}{r_{ij}} - \sum_i U(r_i) \right) + h . \tag{6}$$

The choice of the central potential $U(r)$ is in principle arbitrary, but in order to achieve reasonable convergence, it is important to choose the potential with some care. We shall return to this question in Sec. VI.

The eigenfunctions of H_0 are used to partition the Hilbert space into two parts which we shall call the *model space* (D) and the *orthogonal space* (Q). The partitioning is assumed to be made in such a way that degenerate eigenfunctions of H_0 all belong to the same subspace. In our case H_0 is a central-field Hamiltonian, and its eigenvalues may be characterized by giving the principal quantum numbers n and l of the electrons. The model space then consists of all states of one or several configurations. For instance, in the first calculation reported in this paper the model space consists of the six states of the $1s^2 2p$ configuration. All other states belong to the orthogonal space.

The basic idea of the effective-operator approach is to transform the full Hamiltonian, H, operating on the entire Hilbert space, into an "effective" Hamiltonian H_{eff} operating only on the model space. The problem of finding some of the energies of the system is then reduced to diagonalizing a finite matrix.

In this section we shall give a perturbation expansion of the effective Hamiltonian. In the following sections we will show how this operator can be represented graphically and evaluated using the solutions of inhomogeneous differential equations.

We shall first consider the problem of constructing a suitable effective operator. The projection operators for the model and orthogonal space are

$$P = \sum_{a \in D} |a\rangle\langle a| \quad \text{and} \quad Q = 1 - P = \sum_{r \notin D} |r\rangle\langle r| , \tag{7}$$

respectively. Obviously, these operators commute with the model Hamiltonian,

$$[P, H_0] = [Q, H_0] = 0 . \tag{8}$$

If we operate on the Schrödinger equation

$$(E^\alpha - H_0)\Psi^\alpha = V\Psi^\alpha \tag{9}$$

from the left with P and Q, respectively, we obtain

$$(E^\alpha - H_0)P\Psi^\alpha = PV\Psi^\alpha , \tag{10a}$$

$$(E^\alpha - H_0)Q\Psi^\alpha = Q V\Psi^\alpha \ . \tag{10b}$$

The projection of the true wave function Ψ^α onto the model space is called the *model function*:

$$\Psi_0^\alpha = P\Psi^\alpha \ . \tag{11}$$

Equation (10b) can be solved formally by means of the *resolvent*,

$$T^\alpha = Q/(E^\alpha - H_0) \ , \tag{12}$$

giving

$$Q\Psi^\alpha = T^\alpha V\Psi^\alpha \quad \text{or} \quad \Psi^\alpha = \Psi_0^\alpha + T^\alpha V\Psi^\alpha \ . \tag{13}$$

This leads directly to the Brillouin-Wigner (BW) expansion

$$\Psi^\alpha = (1 + T^\alpha V + T^\alpha V T^\alpha V + \cdots)\Psi_0^\alpha$$

$$= \left(1 + \frac{Q}{E^\alpha - H_0} V + \frac{Q}{E^\alpha - H_0} V \frac{Q}{E^\alpha - H_0} V + \cdots\right)\Psi_0^\alpha \ . \tag{14}$$

If we introduce an operator X^α, satisfying the equation

$$X^\alpha = P + T^\alpha V X^\alpha \ , \tag{15}$$

it follows from (13) that X^α converts the model function Ψ_0^α into the full wave function Ψ^α,

$$\Psi^\alpha = X^\alpha \Psi_0^\alpha \ . \tag{16}$$

$W^\alpha = VX^\alpha$ has the same effect on Ψ_0^α as V has on Ψ, and it is therefore often called the *effective interaction*. By operating on (15) with V from the left, we obtain a reaction type of equation for this interaction,

$$W^\alpha = VX^\alpha = VP + VT^\alpha W^\alpha \tag{17}$$

or

$$W^\alpha = (V + VT^\alpha V + VT^\alpha V T^\alpha V + \cdots)P \ . \tag{18}$$

It can also be given a closed form,[10]

$$W^\alpha = VP + VQ(E^\alpha - QHQ)^{-1} QVP \ . \tag{19}$$

From (10a) it follows that the "effective" Hamiltonian

$$H_{\text{eff}}^\alpha = PH_0P + PW^\alpha \tag{20}$$

satisfies the eigenvalue equation

$$H_{\text{eff}}^\alpha \Psi_0^\alpha = E^\alpha \Psi_0^\alpha \ . \tag{21}$$

This operator acts only within the model space, but it reproduces an *exact* eigenvalue of the full Hamiltonian. The corresponding eigenfunction is equal to the model function (11).

This is the effective Hamiltonian frequently used in nuclear calculations.[20] It has the disadvantage that it depends on the exact energy of the state considered and can therefore be applied only to one energy level at a time.

For many applications it would be of greater interest to have an operator which directly gives the energy *splitting* between certain levels rather than the total energy of a single level. This can be accomplished by means of an effective Hamiltonian, which is independent of the energy within a certain model space. Such an operator has been constructed by Brandow[12] by expanding the energy dependence out of the denominators of the BW perturbation series. As shown by Sandars[18] and one of the present authors,[19] the same results can be derived in a simpler way by starting from the RS expansion, and we shall indicate this treatment here.

As before, the model space (D) is defined by means of the eigenfunctions of a model Hamiltonian H_0 corresponding to one or several eigenvalues (configurations). If the model space has d dimensions, one can show that d of the eigenfunctions of the full Hamiltonian have their zeroth-order limits (when the perturbation is turned off adiabatically) in the model space. The projections of these eigenfunctions onto the model space are the model functions (11)

$$\Psi_0^\alpha = P\Psi^\alpha \quad (\alpha = 1, 2, \ldots, d) \ . \tag{22}$$

We also introduce a *wave operator* Ω which transforms the d model functions into the corresponding eigenfunctions of H,

$$\Psi^\alpha = \Omega\Psi_0^\alpha \quad (\alpha = 1, 2, \ldots, d); \quad \Omega Q = 0 \ . \tag{23}$$

We can illustrate the P and Ω operators in a simple manner as shown in Fig. 1.

Inspection of these diagrams gives directly

$$\Omega P = \Omega \ , \quad P\Omega = P \ . \tag{24}$$

If we operate on the Schrödinger equation (2) from the left with P and use Eqs. (22) and (23), we obtain

$$PH\Omega\Psi_0^\alpha = E^\alpha \Psi_0^\alpha \quad (\alpha = 1, 2, \ldots, d) \ . \tag{25}$$

The effective Hamiltonian

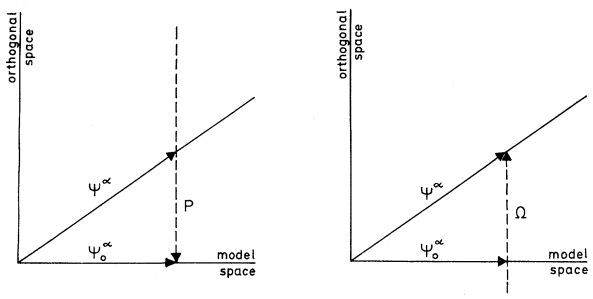

FIG. 1. Pictorial representation of the projection operator P and the wave operator Ω.

$$H_{\text{eff}} = PH\Omega = PH_0P + PV\Omega \tag{26}$$

then satisfies the eigenvalue equation

$$H_{\text{eff}}\,\Psi_0^\alpha = E^\alpha \Psi_0^\alpha \quad (\alpha = 1, 2, \ldots, d)\ . \tag{27}$$

In contrast to the operator (20), this operator is energy independent, and it reproduces all d eigenvalues of the full Hamiltonian that correspond to the states in that space. This implies that if we know the wave operator Ω (with sufficient accuracy), we can obtain the complete level structure corresponding to one or several configurations by solving a single secular equation of finite dimensionality. We shall now indicate how this effective operator can be constructed by means of a linked-diagram expansion.[18,19]

If we operate on (10a) with Ω from the left, we obtain, using (22–24),

$$E^\alpha \Psi^\alpha - \Omega H_0 \Psi_\alpha^0 = \Omega V \Omega \Psi_0^\alpha\ . \tag{28}$$

By means of the Schrödinger equation (9) we can now eliminate the energy E^α, yielding

$$(\Omega H_0 - H_0\Omega)\Psi_0^\alpha = (V\Omega - \Omega V\Omega)\Psi_0^\alpha\ . \tag{29}$$

This equation holds for *all* d states of the model space. In order to obtain a perturbation expansion of Ω we define

$$\Omega = \Omega^{(0)} + \Omega^{(1)} + \Omega^{(2)} + \cdots\ , \tag{30}$$

where $\Omega^{(k)}$ contains k interactions of the perturbation V. This leads to the recursion formula

$$\begin{aligned} &\Omega^{(0)} = P\ , \\ &[\Omega^{(n)}, H_0] = Q V \Omega^{(n-1)} - \sum_{m=1}^{n-1} \Omega^{(n-m)} V \Omega^{(m-1)}\ . \end{aligned} \tag{31}$$

This equation can be solved formally by means of a resolvent S,

$$\Omega^{(n)} = S(V\Omega^{(n-1)}) - S\left(\sum_{m=1}^{n-1} \Omega^{(n-m)} V \Omega^{(m-1)}\right)\ , \tag{32}$$

where S is defined by

$$\langle r|S(A)|a\rangle = \langle r|A|a\rangle\ /(E_0^a - E_0^r)\ . \tag{33}$$

The resolvent thus yields an energy denominator equal to the difference in unperturbed energy between the initial and final states for the operator in the parentheses. The state $|a\rangle$ is here always in the model space and the state $|r\rangle$ is always in the orthogonal space. When the expansion (32) is translated into diagrammatic form, it can be shown that the unlinked diagrams of $V\Omega^{(n-1)}$ cancel the remaining terms, so that only linked (and so-called "folded" or "backward") diagrams remain,

$$[\Omega^{(n)}, H_0] = \{V\Omega^{(n-1)}\}_L \tag{34a}$$

or

$$\Omega^{(n)} = \{S(V\Omega^{(n-1)})\}_L = \{S(VS(VS(V, \ldots)))\}_L P\ . \tag{34b}$$

In the treatment above, we have made no assumption about the energies of the model space. If all states of that subspace are exactly degenerate (with the energy E_0), the formulas above reduce to the more well-known ones. Equation (29) then becomes

$$(E_0 - H_0)\Psi^\alpha = (V\Omega - \Omega V\Omega)\Psi_0^\alpha\ , \tag{35}$$

an equation first derived by Bloch.[17] This can be solved by means of the resolvent

$$R = Q/(E_0 - H_0)\ ,$$

leading to the well-known Rayleigh-Schrödinger expansion. The linked-diagram theorem can then be written

$$\Omega = \sum_{n=0}^{\infty} \left(\frac{Q}{E_0 - H_0}\, V\right)_L^n P\ , \tag{36}$$

which is, for instance, the form used by Kelly.[3] Also the calculations reported in this paper will be based on this form, but in other works to be reported later the more general form of the linked-diagram theorem (34) is used. The diagrams of the effective Hamiltonian (26) are obtained by "closing" the wave-operator diagrams with the perturbation V so that the final state belongs to the model space.

Frequently, one is not primarily interested in the total energy of the system but rather in the effect of some small perturbation h, such as the hyperfine interaction. The effective-operator formalism is also very convenient in this case. It is easy to show that one can obtain the effective operator for such a perturbation by replacing one V interaction at a time by the interaction h in all possible ways, keeping terms linear in h, i.e., using (34b) and (26),

$$\begin{aligned} &h_{\text{eff}}^{(1)} = PhP\ , \\ &h_{\text{eff}}^{(2)} = P\{hS(V) + VS(h)\}_L P\ , \\ &h_{\text{eff}}^{(3)} = P\{hS(VS(V)) + VS(hS(V)) + VS(VS(h))\}_L P\ , \end{aligned} \tag{37}$$

etc.

III. DIAGRAMMATIC REPRESENTATION OF EFFECTIVE OPERATORS

In Sec. II we have given the basic formulas for the linked-diagram expansion of the wave function and the effective Hamiltonian. We shall now outline how the corresponding diagrams are evaluated.

In representing effective operators, it is important to distinguish between *core* orbitals (oc-

cupied in all determinants of the model space, D), *valence* or *open-shell* orbitals (occupied in some but not all determinants of D), and *excited* orbitals (not occupied in any determinants of D). For core and excited orbitals we shall use the ordinary convention of a vertical line with an arrow pointing downward and upwards, respectively. For open-shell electrons we shall use Sandars's convention[18] of a double arrow, normally pointing upward (see Fig. 2).

The interactions are represented in the usual way by horizontal dashed lines, as illustrated in Fig. 3. There is a matrix element associated with each interaction line and a creation and an absorption operator with each outgoing and incoming line, respectively. The potential diagram 3(a) is given by

$$a_\alpha^\dagger \langle \alpha | U | \beta \rangle a_\beta \,, \tag{38}$$

where U is the central potential in Eq. (4). The electrostatic diagram 3(b) is

$$a_\alpha^\dagger a_\beta^\dagger \langle \alpha_1 \beta_2 | 1/r_{12} | \gamma_1 \delta_2 \rangle a_\delta a_\gamma \,, \tag{39}$$

and the hyperfine interaction 3(c) is

$$a_\alpha^\dagger \langle \alpha | h | \beta \rangle a_\beta \,, \tag{40}$$

where h is given by Eq. (1). The diagrams given in Fig. (3) thus show which single-electron states are involved in the interaction, and how these states are joined together in the interaction matrix elements.

According to Eq. (34), the wave-operator diagrams of a given order are obtained from the diagrams of preceding order by operating with SV and joining the lines together in all possible ways. A diagram produced in this way, which has no free lines other than open-shell lines, is said to be *closed*. A diagram, which has a closed part that is not connected, is said to be *unlinked*. The basic LD theorem says that the unlinked diagrams cancel at each order of the perturbation theory. For each interaction, which occurs in a diagram of the wave operator, the resolvent S supplies an energy denominator, which according to Eq. (33) is the energy difference between the state following the interaction and the initial state. These energy denominators E_m may be found by drawing a horizontal line above each interaction line and using the formula

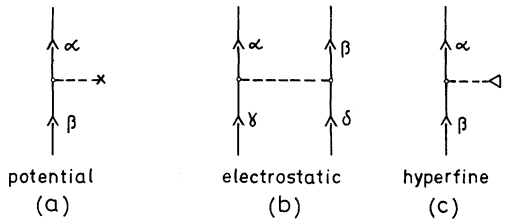

FIG. 3. Graphical representation of the potential, Coulomb, and hyperfine interactions.

$$E_m = \sum (\epsilon_c + \epsilon_o - \epsilon_e) \,, \tag{41}$$

where ϵ_c and ϵ_e are the single-particle energies of, respectively, the down-going and up-going lines cut by our imaginary horizontal line, and ϵ_o are the energies of the incoming open-shell lines.

Any diagram obtained by successively applying SV, which is linked at each order of the perturbation theory, is allowed. It will have the property that the intermediate states, which occur above each interaction line, are orthogonal to the model space. Since the wave operator Ω operates to the right only on the model space, it follows that there can be no free lines other than open-shell lines at the bottom of a diagram. According to Eq. (26), the corresponding effective-operator diagrams are obtained by "closing" the diagrams of the wave operator by a final interaction. So only open-shell lines may appear as free *out-going* lines. The effective-operator diagrams must then be of the schematic form shown in Fig. 4, where the box represents a diagrammatic part with no free lines and no intermediate states within the model space.

An effective-operator diagram with n incoming and n outgoing lines is said to represent an effective *n-body operator*. Evidently, any effective operator can be separated into zero-body, one-body, two-body, etc. parts. For the atomic states, which we shall consider in this paper, there is only one electron in the open shell, and so only the zero-body and one-body operators have nonzero

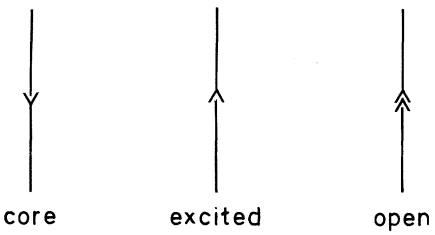

FIG. 2. Directed lines corresponding to core, excited, and open-shell orbitals.

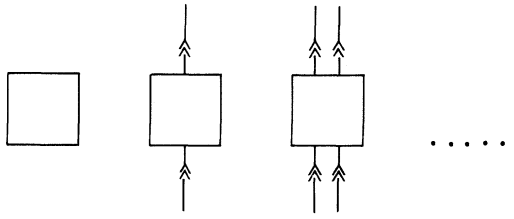

FIG. 4. Graphical representation of zero, one-, and two-body effective operators.

matrix elements. Of these, the zero-body operators are independent of the azimuthal quantum numbers and give no hyperfine splitting. Therefore, we shall in the following consider only one-body effective operators. Since a one-body tensor operator is determined, apart from a radial factor, by its ranks in the spin and orbital spaces, the one-body part of the effective operator is also of the form (1). Thus higher-order effects may be incorporated into the ordinary hyperfine operator by modifying the $\langle r^{-3}\rangle$ values associated with the different terms.

Each effective-operator diagram is made up of three elements: creation and absorption operators, a phase, and one- and two-particle matrix elements. In addition, all diagrams have associated with them an energy denominator given by Eq. (41) for each interaction line, except the last one. The first-order diagram, which represents the hyperfine interaction within the model space, and the four second-order diagrams are shown in Fig. 5.

The effective operator corresponding to the first-order diagram 5(a) is

$$a_p^\dagger a_o \langle p|h|o\rangle \ , \tag{42}$$

where p and o stand for the open-shell quantum numbers $p=(n^p l^p m_s^p m_l^p)$, $o=(n^o l^o m_s^o m_l^o)$ and h is given by Eq. (1). In the second-order diagrams, the states a are core orbitals, while the i are excited states in 5(c) and may either be an excited or open-shell state in 5(d) and 5(e). The special symbol, ---⊗, corresponds to the interaction of an orbital with the central potential and with the spherical average of the direct and exchange interactions. The effect of this interaction upon the open-shell orbitals is shown schematically in Fig. 6.

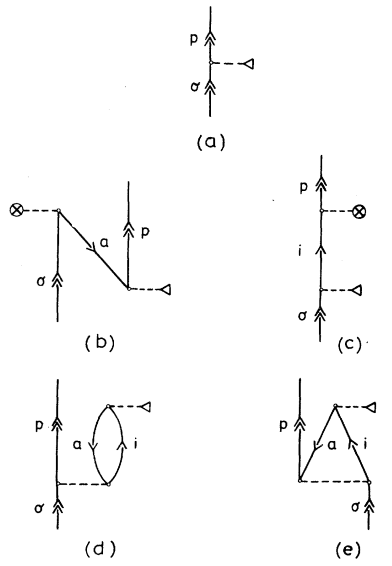

FIG. 5. First- and second-order Feynman diagrams that contribute to the hyperfine interaction.

Again, for the atomic states which we shall consider in this paper, there is only one electron in the open-shell, and so the sums over n and l include only closed-shell states. For states having two or more electrons in the open shell, the effective operators which depend upon the coordinates of several electrons may be evaluated explicitly. It is probably best, however, to choose a potential for such cases that includes the largest part of the two-body effects. If we denote the one-body potential operator, which corresponds to each interaction line, ----⊗, by v, then the explicit expression for diagram 5(b) is

$$-\sum_a a_p^\dagger a_o \frac{\langle p|h|a\rangle\langle a|v|o\rangle}{(\epsilon_a-\epsilon_p)} \ , \tag{43}$$

and for 5(c),

$$\sum_i a_p^\dagger a_o \frac{\langle p|v|i\rangle\langle i|h|o\rangle}{(\epsilon_o-\epsilon_i)} \ . \tag{44}$$

The minus sign that occurs in (43) is due to the fact that the diagram 5(b) contains one hole line. As in the Brueckner-Goldstone formalism,[1-3] a phase factor $(-1)^{h+l}$ is associated with each diagram, where h is the number of hole lines and l the number of closed loops. In addition, there is a special phase rule for backward diagrams, which we shall not consider here.[18,19] Further discussion of the potential diagrams 5(b) and 5(c) will be postponed until Sec. V, which deals with the inhomogeneous one- and two-electron equations. These diagrams together with all third-order diagrams involving potential interactions may automatically be taken into account by successively solving the associated differential equations.

At the first interaction line of diagrams 5(d) and 5(e) a core orbital is excited into another degree of freedom due to an interaction with a state in the unsymmetric valence shell. These diagrams thus correspond to a polarization of the core, and they give a first-order correction to the ordinary hyperfine interaction. The mathematical expression for 5(d) is

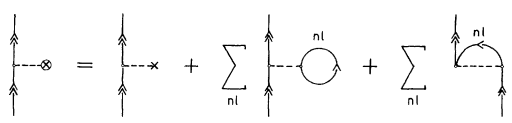

Fig. 6. Diagrams which represent the potential, direct, and exchange interactions.

$$\sum_{a,i} \frac{a_p^\dagger a_o \langle a|h|i\rangle\langle pi|1/r_{12}|oa\rangle}{\epsilon_a - \epsilon_i + \epsilon_o - \epsilon_p} \quad . \tag{45}$$

Similarly, for 5(e) we have

$$-\sum_{a,i} \frac{a_p^\dagger a_o \langle a|h|i\rangle\langle pi|1/r_{12}|ao\rangle}{\epsilon_a - \epsilon_i + \epsilon_o - \epsilon_p} \quad . \tag{46}$$

As mentioned, we shall in the present article consider only atoms with a single open shell for which $\epsilon_o = \epsilon_p$. For future reference, however, we have given the more general expression above, valid also in the case of several open shells.

The contributions to the effective operators (45) and (46), which are due to the excitations from a single core orbital n_a, l_a to each orbital symmetry l_i, may be considered separately. For given n_a, l_a, l_i, these operators have the form

$$\sum_{n_i} \frac{a_p^\dagger a_o \langle a|h|i\rangle\langle pi|1/r_{12}|oa\rangle}{\epsilon_a - \epsilon_i + \epsilon_o - \epsilon_p} \tag{47}$$

and

$$-\sum_{n_i} \frac{a_p^\dagger a_o \langle a|h|i\rangle\langle pi|1/r_{12}|ao\rangle}{\epsilon_a - \epsilon_i + \epsilon_o - \epsilon_p} \quad . \tag{48}$$

The third-order diagrams may conveniently be divided into correlation and core-polarization diagrams. We shall refer to any diagram as a correlation diagram that contains an interaction line at which two electrons are excited from the core or open shell into excited states. This seems to correspond to the intuitive idea of correlation, since a diagram of this kind describes a physical process in which two electrons in the sea of occupied states move out into other degrees of freedom due to their mutual Coulomb interaction. The core-polarization diagrams that occur at third order represent a second-order correction to the hyperfine interaction. They have a single excited state at a time and, as we shall see, they may be evaluated using only single particle perturbed functions. These diagrams correspond to relaxing the restriction that the single-particle wave functions are of the form (5), and they are thus implicitly included in the unrestricted Hartree-Fock procedure. Apart from diagrams involving the potential interaction, there are four third-order core-polarization diagrams and twenty-four correlation diagrams for which the hyperfine interaction occurs last. These diagrams are shown in Figs. 7 and 8, respectively. They may be evaluated by writing down the matrix element and energy denominator corresponding to each interaction line and including a phase factor according to the general rule discussed above. In order to illustrate this, we have shown the diagrams 7(a) and 8(a) in more detail in Fig. 9.

The effective operator corresponding to Fig. 9(a) is (for $\epsilon_o = \epsilon_p$)

$$-\sum_{n_i, n_j} \frac{a_p^\dagger a_o \langle b|h|j\rangle\langle aj|1/r_{12}|bi\rangle\langle pi|1/r_{12}|oa\rangle}{(\epsilon_a - \epsilon_i)(\epsilon_b - \epsilon_j)} \quad , \tag{49}$$

and the operator corresponding to Fig. 9(b) is

$$\sum_{n_i, n_j, n_k} \frac{a_p^\dagger a_o \langle p|h|k\rangle\langle ka|1/r_{12}|ij\rangle\langle ij|1/r_{12}|oa\rangle}{(\epsilon_o - \epsilon_k)(\epsilon_o + \epsilon_a - \epsilon_j - \epsilon_i)} \quad . \tag{50}$$

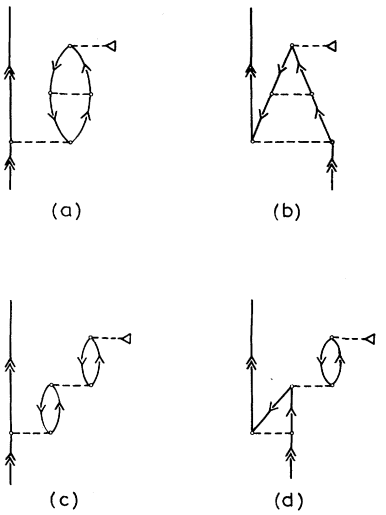

FIG. 7. Third-order core-polarization diagrams.

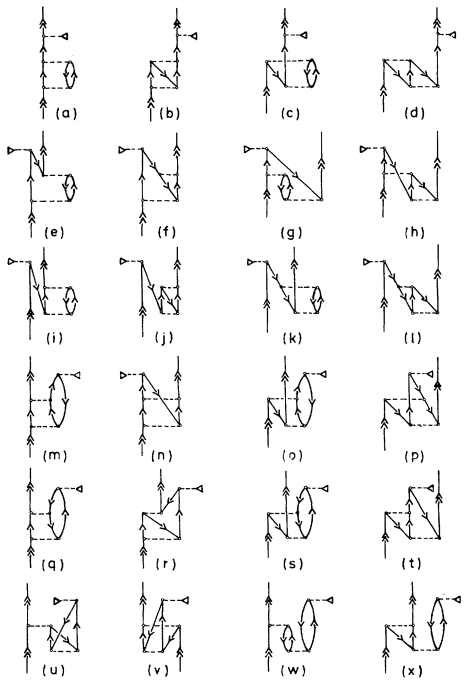

FIG. 8. Third-order correlation diagrams.

In addition to the third-order diagrams shown in Figs. 7 and 8 and to the diagrams obtained from them by reflection in a horizontal plane, there are diagrams for which the hyperfine interaction occurs between the two Coulomb interaction. Eighteen distinct diagrams may be obtained by interchanging the order of the hyperfine and Coulomb interactions in this way. As we shall see, the matrix elements which occur in the explicit expressions for the Feynman diagrams have a radial part and an angular factor. The angular factors are independent of the ordering of the hyperfine and Coulomb interactions in the diagram. There are thus eighteen different angular factors corresponding to the third-order core-polarization and correlation diagrams, and in all there are 46 distinct diagrams. We will discuss the physical significance of the most important third-order diagrams in Sec. VI.

IV. EVALUATION OF THE ANGULAR FACTORS

All of the operators which appear in the hyperfine interaction (1) have an electronic and a nuclear part. The electronic part of the quadrupole interaction, $r^{-3}C_q^{(2)}$, and the spin-dipole (sd) interaction, $r^{-3}(\vec{s}\vec{C}^{(2)})_Q^{(1)}$, are quite similar, and so they will provide useful examples of our method. The spin and orbital parts of the sd interaction are coupled together to form a vector in the total space:

$$r^{-3}(sC^{(2)})_Q^{(1)} = r^{-3}\sum_{q',q}(1q'2q|1Q)s_{q'}C_q^{(2)} .$$

We shall find that the effect of an interaction of the form

$$r^{-3}s_{q'}t_q^{(k)} \tag{51}$$

upon the model space can be represented by an effective operator

$$cs_{q'}t_q^{(k)} ,$$

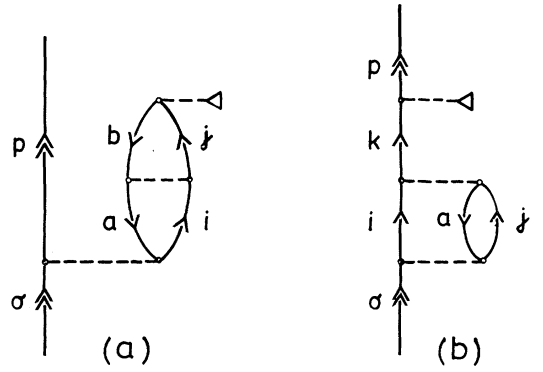

FIG. 9. Example of a third-order core-polarization diagram and a third-order correlation diagram.

where c is independent of q. The spin and orbital operators appear on the same footing in $r^{-3}s_{q'}t_q^{(k)}$ and so c is also independent of q'. It follows that the coefficient $(1q'2q|1Q)$, which couples the spin and orbital parts of the spin-dipole interaction, carries through the evaluation of the Feynman diagrams, and we may evaluate the effect of an uncoupled operator of the form (51). For the purposes of calculating diagrams, it is also convenient to choose $q' = 0$. Then the operator (51) is of the general form

$$f(r)s_z^\kappa t_q^{(k)} , \tag{52}$$

where κ and k are the ranks of the operator in the spin and orbital spaces and where we have used the natural notation

$$s_z^0 = 1, \quad s_z^1 = s_z .$$

The other components of the hyperfine interaction also are of the general form (52), and so is the spin-orbit interaction and the interaction of the electrons with an external field.

The basic LD theorem represents the effect of the perturbation by a series of diagrams, each of which corresponds to a fundamental physical process. The matrix elements which occur in the explicit expression of these diagrams may also be written graphically. The orbital part of the matrix element of operator (52) is

$$\langle n_\alpha l_\alpha m_l^\alpha|f(r)t_q^{(k)}|n_\beta l_\beta m_l^\beta\rangle = \langle n_\alpha l_\alpha|f(r)|n_\beta l_\beta\rangle \times\langle l_\alpha m_l^\alpha|t_q^{(k)}|l_\beta m_l^\beta\rangle , \tag{53}$$

and we may use the Wigner-Eckart theorem and the symmetry properties of the 3-j symbols to write the matrix element of $t_q^{(k)}$:

$$\langle l_\alpha m_l^\alpha|t_q^{(k)}|l_\beta m_l^\beta\rangle = (-1)^{l_\alpha - m_l^\alpha}\langle l_\alpha||t^{(k)}||l_\beta\rangle F , \tag{54}$$

where F is the angular-momentum diagram given in Fig. 10(a). This diagram corresponds to the 3-j symbol

$$\begin{pmatrix} l_\alpha & l_\beta & k \\ m_l^\alpha & -m_l^\beta & -q \end{pmatrix} . \tag{55}$$

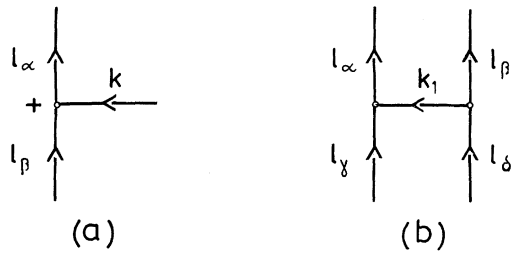

FIG. 10. The angular-momentum diagrams corresponding to a one-body tensor operator and to the Coulomb interaction.

The direction of each arrow in an angular-momentum diagram of this kind indicates the sign of the corresponding magnetic quantum number in the 3-j symbol. A line directed away from the junction corresponds to the positive sign of the magnetic quantum number and a line directed toward the junction to the negative sign. In order to define a 3-j symbol uniquely, it is also necessary to specify the order of the angular momentum occurring in the symbol. The positive sign near the juncture of Fig. 10(a) means that the angular momenta in the 3-j symbol (55) are orientated in a counterclockwise fashion in the diagram. A negative sign would mean they had a clockwise orientation.

The electrostatic matrix element is given by

$$\langle \alpha_1\beta_2|1/r_{12}|\gamma_1\delta_2\rangle = (-1)^{l_\alpha - m_l^\alpha}(-1)^{l_\beta - m_l^\beta}\delta(m_s^\alpha, m_s^\gamma)\,\delta(m_s^\beta, m_s^\delta)\sum_{k_1}[(-1)^{k_1}(l_\alpha||C^{(k_1)}||l_\gamma)(l_\beta||C^{(k_1)}||l_\delta)R^{k_1}(\alpha\beta\gamma\delta)]G\,, \tag{56}$$

where $R^{k_1}(\alpha\beta\gamma\delta)$ is an ordinary Slater integral and G is the angular momentum diagram shown in Fig. 10(b). The diagram corresponds to the expression

$$\sum_{q_1}(-1)^{k_1-q_1}\begin{pmatrix} l_\alpha & l_\gamma & k_1 \\ m_l^\alpha & -m_l^\gamma & -q_1\end{pmatrix}\begin{pmatrix} l_\beta & l_\delta & k_1 \\ m_l^\beta & -m_l^\delta & q_1\end{pmatrix}. \tag{57}$$

The sum of the angular momenta which occur in each 3-j symbol is even, and so the 3-j symbols are independent of the ordering of the angular momenta. For this reason, we have not written a sign by the two junctures of the diagram shown in Fig. 10(b). In what follows, we shall denote the product of $(-1)^{k_1}$ and the reduced matrix elements that appear in Eq. (56) by the special symbol $X(k_1, \alpha\beta\gamma\delta)$. We then have

$$X(k, \alpha\beta\gamma\delta) = (-1)^k(l_\alpha||C^{(k)}||l_\gamma)(l_\beta||C^{(k)}||l_\delta), \tag{58}$$

and the Coulomb matrix elements are of the simple form

$$\langle \alpha_1\beta_2|1/r_{12}|\gamma_1\delta_2\rangle = (-1)^{l_\alpha - m_l^\alpha}(-1)^{l_\beta - m_l^\beta}\delta(m_s^\alpha, m_s^\gamma) \times \delta(m_s^\beta, m_s^\delta) \times \sum_{k_1} X(k_1, \alpha\beta\gamma\delta)R^{k_1}(\alpha\beta\gamma\delta)G\,, \tag{59}$$

where G is shown in Fig. 10(b).

Using Eqs. (54) and (59), the orbital part of the hyperfine matrix elements and the Coulomb interaction may be represented by angular-momentum diagrams. There is, in addition, a phase factor $(-1)^{l-m_l}$ associated with each outgoing line and a factor which is characteristic of the interaction. For the hyperfine interaction this factor is just

$$\langle n_\alpha l_\alpha|r^{-3}|n_\beta l_\beta\rangle\langle l_\alpha||t^{(k)}||l_\beta\rangle,$$

while for the Coulomb matrix elements, it is

$$X(k_1, \alpha\beta\gamma\delta)R^{k_1}(\alpha\beta\gamma\delta).$$

Since the Coulomb interaction is spin-independent, the matrix element (59) also has a spin δ function associated with each vertex of the angular-momentum diagram. Both the contact $\delta(\vec{r})\vec{s}$ and the spin-dipole operator $r^{-3}(\vec{s}\vec{C}^{(2)})^{(1)}$, however, depend upon spin. The matrix of the contact term and the spin part of an operator (52) with $\kappa = 1$ is just

$$\langle \tfrac{1}{2} m_s^\alpha|s_z|\tfrac{1}{2} m_s^\beta\rangle = m_s^\alpha\delta(m_s^\alpha, m_s^\beta).$$

The angular part of the perturbation diagrams may be evaluated in a very elegant way by taking advantage of the fact that the Feynman diagrams which correspond to the hyperfine and Coulomb interactions are identical to the angular-momentum diagrams which describe their respective matrix elements. The Feynman diagrams of these interactions are given in Fig. 3 and the corresponding angular-momentum diagrams are shown in Fig. 10. As we have said, the higher-order diagrams in the perturbation expansion may be formed by operating successively with SV [Eq. (34b)] and joining the lines together to form linked diagrams. This procedure may also be applied to the associated orbital angular-momentum diagrams. When two lines are joined together, this corresponds to summing over the azimuthal quantum numbers m_s and m_l that occur in two matrix elements. These quantum numbers in turn are associated with the free ends of two lines of the angular-momentum diagrams that describe the matrix elements, and the additional phase factor $(-1)^{l-m}$ is necessary to accomplish the summation graphically.[21] The matrix elements which occur in the expressions for the effective operator thus have a radial part, an orbital-angular momentum part that can be represented by a diagram topologically equivalent to the Feynman diagram, and there is in addition a spin sum. The diagonal matrix elements of s_z are $+\frac{1}{2}$ and $-\frac{1}{2}$. So if a spin-dependent interaction modifies a closed loop, the summation over the spin quantum numbers will produce a null result. For the Coulomb interaction or a spin-independent single-particle operator, however, the spin sum multiplies the contribution from a given diagram

by a factor of 2 for each string which does not contain any free valence shell lines.

The evaluation of effective operators has been treated in some detail by Sandars.[18] Apart from our method of implicitly including the potential diagrams, the only novel feature of this work is the manner in which the radial part of the diagrams is evaluated. So we will content ourselves with a few examples. For a general operator of the form (52), the radial part of the second-order diagram (47) may be written

$$R_1^{(k_1)} = \sum_{n_i} \frac{\langle n_a l_a | f(r) | n_i l_i \rangle R^{k_1}(nln_i l_i, nln_a l_a)}{\epsilon_a - \epsilon_i} \quad (60a)$$

for a single open shell (nl), and the radial part of the operator (48) is

$$R_2^{(k_1)} = \sum_{n_i} \frac{\langle n_a l_a | f(r) | n_i l_i \rangle R^{k_1}(nln_i l_i, n_a l_a nl)}{\epsilon_a - \epsilon_i} . \quad (60b)$$

Here the sum n_i includes both the bound and continuum excited states. Much of the numerical work in a perturbative calculation is usually concerned with solving for a complete set of single-particle states. Instead of constructing the excited states explicitly, however, the radial factors may be written in terms of one- and two-electron perturbed functions which satisfy a differential equation. This technique which greatly simplifies the calculation will be discussed in Sec. V.

The orbital part of the matrix elements of the effective operator (47), which corresponds to diagram 5(d), may be written

$$\langle l_a || t^{(k)} || l_i \rangle X(k_1, ll_i ll_a) H_{p,o} , \quad (61a)$$

where $H_{p,o}$ is the angular-momentum diagram shown in Fig. 11(a), and the operator (48), which corresponds to 5(e), has an orbital part

$$\langle l_a || t^{(k)} || l_i \rangle X(k_1, ll_i l_a l) K_{p,o} , \quad (61b)$$

where $K_{p,o}$ appears in Fig. 11(b). Collecting together the radial factor (60a) and the orbital part of the matrix elements given by (61a), the effective operator (47) may be written

$$2\delta_{\kappa 0} \langle l_a || t^{(k)} || l_i \rangle \sum_{k_1} X(k_1, ll_i ll_a) R_1^{(k_1)} a_p^\dagger a_o H_{p,o} . \quad (62)$$

Here the factor $2\delta_{\kappa 0}$ comes from the spin sum and $R_1^{(k_1)}$ includes the effect of all excited states n_i. Similarly, using (60b) and (61b), the effective operator (48) may be written as

$$\langle l_a || t^{(k)} || l_i \rangle \sum_{k_1} X(k_1, ll_i l_a l) R_2^{(k_1)} a_p^\dagger a_o K_{p,o} . \quad (63)$$

We turn now to the problem of evaluating the angular momentum diagrams $H_{p,o}$ and $K_{p,o}$.

The direction of any line in an angular-momentum graph may be reversed, provided that the line is joined at both ends and corresponds to an integer value of the angular momentum. So the two diagrams shown in Fig. 11 may be reduced using the graphical identities given in Fig. 12(a) and 12(b). This reduction is shown in Fig. 12(c) and 12(d). Using the graphical representation of the Wigner-Eckart theorem (54) and the expression for $H_{p,o}$ given in 12(c), the operator (62) assumes the form

$$2\delta_{\kappa 0} \langle l_a || t^{(k)} || l_i \rangle X(k, ll_i ll_a) \times R_1^{(k)} [(2k+1) \langle l || t^{(k)} || l \rangle]^{-1} a_p^\dagger a_o \langle p | t_q^{(k)} | o \rangle . \quad (64)$$

When a sum is performed over all the open-shell states, the operator

$$\sum_{p,o} a_p^\dagger a_o \langle p | t_q^{(k)} | o \rangle$$

which occurs in (64) is just the second-quantized form of the one-body operator

$$\sum_i t_{iq}^{(k)}$$

acting within the model space. So the effect of the second-order Feynman diagram 5(d), which has the explicit form (47), is to modify the expectation value of $f(r)$ within the model space. The contribution of this diagram is

$$\delta \langle f \rangle = 2\delta_{\kappa 0} \langle l_a || t^{(k)} || l_i \rangle X(k, ll_i ll_a) \times R_1^{(k)} [(2k+1) \langle l || t^{(k)} || l \rangle]^{-1} . \quad (65)$$

Similarly, using the explicit expression for $K_{p,o}$ given in 12(d), the effective operator (63) may be written in the form

$$(-1)^k (\langle l_i || t^{(k)} || l_a \rangle / \langle l || t^{(k)} || l \rangle) \times \sum_{k_1} X(k_1, ll_i l_a l) \begin{Bmatrix} l & l & k \\ l_a & l_i & k_1 \end{Bmatrix} R_2^{(2)} a_p^\dagger a_o \langle p | t_q^{(k)} | o \rangle , \quad (66)$$

and the contribution of the diagram 5(e) is thus

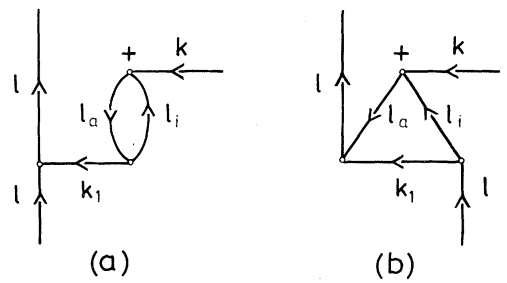

FIG. 11. Angular-momentum diagrams corresponding to the second-order direct and exchange excitations.

$$\delta\langle f\rangle = (-1)^k(\langle l_i||t^{(k)}||l_a\rangle/\langle l||t^{(k)}||l\rangle)\sum_{k_1} X(k_1, l\,l_i l_a\,l)\begin{Bmatrix} l & l & k \\ l_a & l_i & k_1 \end{Bmatrix} R_2^{(2)} . \tag{67}$$

The third-order diagram may also be evaluated in this way. For instance, the radial part of the effective operator (49) (Fig. 9a) is

$$R_1^{(k_1,k_2)} = \sum_{n_i,n_j} \frac{\langle n_b l_b|f(r)|n_j l_j\rangle R^{(k_1)}(n_a l_a n_j l_j, n_b l_b n_i l_i) R^{(k_2)}(nln_i l_i, nln_a l_a)}{(\epsilon_a-\epsilon_i)(\epsilon_b-\epsilon_j)} , \tag{68}$$

and the orbital part is represented by the angular-momentum diagram shown in Fig. 13(a). This diagram, which may readily be obtained from the Feynman diagram 9(a), may be evaluated by using the graphical identities given in Fig. 12 to remove first a triangle and then the resulting loop. In this way, the contribution of (49) may be shown to be

$$\delta\langle f\rangle = -2\delta(\kappa,0)\langle l_b||t^k||l_j\rangle[(2k+1)\langle l||t^k||l\rangle]^{-1}\sum_{k_1}\begin{Bmatrix} k & l_i & l_a \\ k_1 & l_b & l_j \end{Bmatrix} X(k_1, l_a l_j l_b l_i) X(k, l_i l\, l_a l) R_1^{(k_1 k)} . \tag{69}$$

Similarly, the radial part of the effective operator (50) (Fig. 9b) is

$$R_2^{(k_1k_2)} = \sum_{n_i,n_j,n_k} \frac{\langle nl|f(r)|n_k l_k\rangle R^{(k_1)}(n_k l_k n_a l_a, n_i l_i n_j l_j) R^{(k_2)}(n_i l_i n_j l_j, nln_a l_a)}{(\epsilon_0-\epsilon_k)(\epsilon_0+\epsilon_a-\epsilon_j-\epsilon_i)} , \tag{70}$$

and the orbital part is represented by the diagram shown in Fig. 13(b). This diagram may be evaluated by applying the graphical identity 12(a) successively to remove the two loops. The result is

$$\delta\langle f\rangle = \frac{2\delta(l_k, l)}{2l+1}\sum_{k_1}\frac{X(k_1, l_k l_a l_i l_j) X(k_1, l_i l_j l\, l_a) R_2^{(k_1 k_1)}}{2k_1+1} . \tag{71}$$

V. EVALUATION OF RADIAL FACTORS

A. General treatment

In Sec. IV we have seen how the spin-angular part of the effective-operator diagrams can conveniently be evaluated by means of angular-momentum diagrams. What remains to be calculated is thus the radial part, including the energy denominators. As we have said, this can be accomplished in essentially two different ways. One is to use a complete set of orbitals and explicitly evaluate sums of the kind (60) and (68), as done, for instance, by Kelly.[3] The other is to solve one- and two-particle equations for the particular linear combination of excited states that contribute

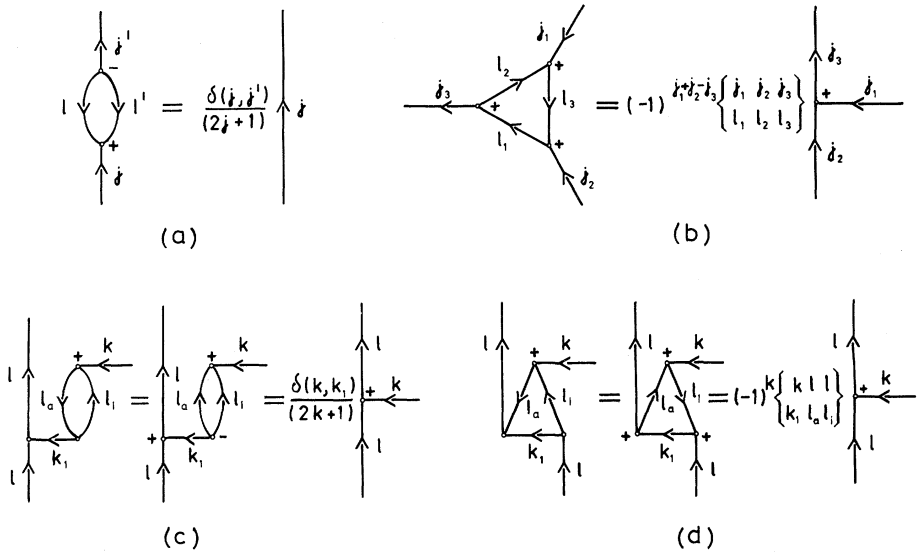

FIG. 12. Graphical identities for the reduction of second-order angular-momentum diagrams.

to the Feynman diagrams. One-particle equations of this kind have been used for a long time by Sternheimer[22] to calculate the effect of quadrupole shielding. Recently, accurate finite-difference methods have become available for solving such two-particle equations,[23] and they have been applied recently to perturbative calculations by Schulman and Lee[27] and by Morrison.[26]

The basic idea of the use of inhomogeneous differential equations in perturbation theory can be simply described in the following way. Let us consider the first-order equation (31)

$$[\Omega^{(1)}, H_0] = QVP , \tag{72}$$

where

$$\Psi^{(1)} = \Omega^{(1)}\Psi_0$$

is the first-order wave function. This equation can be solved by means of the resolvent technique, described in Sec. II, which leads to the ordinary perturbation expansion. Alternatively, we can consider Eq. (72) as an inhomogeneous differential equation and solve it as such. We shall consider this approach here.

Since we are, in the present work, particularly interested in the hyperfine interaction, we shall assume that there is a small perturbation h in addition to the electrostatic interaction V. We can then separate the first-order wave function or wave operator into two parts, satisfying the equations

$$[\Omega_v^{(1)}, H_0] = QVP , \tag{73a}$$

$$[\Omega_h^{(1)}, H_0] = QhP , \tag{73b}$$

$$\Psi_v^{(1)} = \Omega_v^{(1)}\Psi_0; \quad \Psi_h^{(1)} = \Omega_h^{(1)}\Psi_0 . \tag{73c}$$

Using the "intermediate normalization"

$$\langle\Psi_0|\Psi_0\rangle = \langle\Psi_0|\Psi\rangle = 1 ,$$

the energy contribution due to the interaction h becomes

$$E_h = \langle\Psi_0|h_{\text{eff}}|\Psi_0\rangle , \tag{74}$$

where the effective operator, h_{eff}, is given by (37). It is then easy to show that the contribution to E_h to third order can for a degenerate model space be expressed entirely by means of the first-order functions defined in (73),

$$\begin{aligned} E_h^{(1)} &= \langle\Psi_0|h|\Psi_0\rangle , \\ E_h^{(2)} &= \langle\Psi_0|h|\Psi_v^{(1)}\rangle + \langle\Psi_0|V|\Psi_h^{(1)}\rangle , \\ E_h^{(3)} &= \langle\Psi_h^{(1)}|V|\Psi_v^{(1)}\rangle + \langle\Psi_v^{(1)}|h|\Psi_v^{(1)}\rangle + \langle\Psi_v^{(1)}|V|\Psi_h^{(1)}\rangle . \end{aligned} \tag{75}$$

If there are several energy levels in the model space, essentially the same result holds, only with a slight modification of the energy denominators.

Since V is a two-body operator, Eq. (73a) leads to one- and two-particle equations, while Eq. (73b), assuming h to be a one-body operator, leads to a one-particle equation. We shall now indicate how these equations can be derived.

B. Derivation of the one- and two-particle equations

We assume that the model space consists of a number of Slater determinants, $A, B, \ldots$, which are not necessarily degenerate in zeroth order. We shall let A_a^i denote a single substitution, i.e., where an orbital a in A is replaced by another orbital i, and, similarly, for double substitutions, A_{ab}^{ij}. These notations agree essentially, for instance, with those used by Nesbet.[4]

We consider first *single* excitations and operate on Eq. (72) with $\langle A_a^i|$ from the left and with $|A\rangle$ from the right, yielding

$$\langle A_a^i|[\Omega^{(1)}, H_0]|A\rangle = \langle A_a^i|QVP|A\rangle ,$$

or

$$(\epsilon_a - \epsilon_i)\langle A_a^i|\Omega^{(1)}|A\rangle = \langle A_a^i|QVP|A\rangle .$$

Let us now define a single-electron function

$$\eta = \sum_i |i\rangle\langle A_a^i|\Omega^{(1)}|A\rangle = \sum_i |i\rangle \frac{\langle A_a^i|QVP|A\rangle}{\epsilon_a - \epsilon_i} , \tag{76}$$

where the summation is performed over all orbitals including those which lie in the continuum. It then follows that this function satisfies the equation

$$(\epsilon_a - h^0)\eta = \sum_i |i\rangle\langle A_a^i|QVP|A\rangle , \tag{77}$$

where h^0 is the single-electron part of H_0 given by Eq. (4).

The "perturbed function" η contains all first-order perturbations due to single excitations from the orbital a. Thus, instead of explicitly evaluating the sum (76), we can solve the inhomogeneous dif-

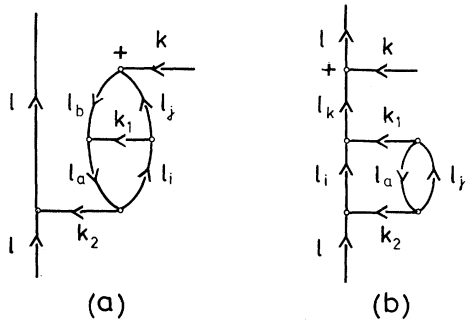

FIG. 13. Angular-momentum diagram corresponding to third-order core-polarization and correlation effects.

ferential equation (77). η is formally related to the corresponding part of the wave operator by $|A_a^\eta\rangle\langle A|$, where in A_a^η the orbital a has been replaced by the perturbed function η.

If the perturbation is a one-body operator of type (52) and the states A_a^i lie in the orthogonal space ($A_a^i \in Q$), then the matrix elements which occur in Eqs. (76) and (77) may be separated into angular and radial parts in the following way:

$$\langle A_a^i|Q\,VP|A\rangle = \langle A_a^i|Q\,VP|A\rangle_{\rm ang}\langle A_a^i|Q\,VP|A\rangle_{\rm rad} = \langle A_a^i|Q\,VP|A\rangle_{\rm ang}\langle n_i l_i|f(r)|n_a l_a\rangle \ . \quad (78)$$

Equation (76) may then be written

$$\eta = \sum_i |i\rangle\langle A_a^i|Q\,VP|A\rangle_{\rm ang}\frac{\langle n_i l_i|f(r)|n_a l_a\rangle}{\epsilon_a - \epsilon_i} \ . \quad (79)$$

It follows from Eqs. (78) and (79) that the angular factors on both sides of Eq. (77) cancel and that the *radial* function

$$\rho_f(n_a l_a \to l_i\,; r) = \sum_{\text{exc } n_i} P_i(r)\frac{\langle n_i l_i|f(r)|n_a l_a\rangle}{\epsilon_a - \epsilon_i} \quad (80)$$

satisfies the equation

$$(\epsilon_a - h_r^0)\rho_f(n_a l_a \to l_i\,; r) = \sum_{\text{exc } n_i} P_i(r)\langle n_i l_i|f(r)|n_a l_a\rangle \ , \quad (81)$$

where

$$h_r^0 = -\frac{1}{2}\frac{d^2}{dr^2} - \frac{Z}{r} + U(r) + \frac{l_i(l_i+1)}{2r^2} \ .$$

We have here used the short-hand notation "exc n_i" for states satisfying the condition $A_a^i \in Q$, and we shall use "occ n_i" for all the rest. The perturbed function (80) describes the mixing of excited states into the core orbital a by means of a one-particle interaction.

We may use the closure relation

$$\delta(r-r') = \sum_{\text{all } n_i} P_i(r)P_i(r') = \sum_{\text{exc } n_i} P_i(r)P_i(r') + \sum_{\text{occ } n_i} P_i(r)P_i(r') \quad (82)$$

to eliminate the excited states from Eq. (81). In this way, we obtain the inhomogeneous equation

$$(\epsilon_a - h_r^0)\rho_f(n_a l_a \to l_i\,; r) = f(r)P_a(r) - \sum_{\text{occ } n_i} P_i(r)\langle n_i l_i|f(r)|n_a l_a\rangle \ , \quad (83)$$

which may be solved numerically for $\rho_f(n_a l_a \to l_i\,; r)$. The explicit expression given for this function in Eq. (80) is orthogonal to all of the occupied orbitals. The second term, which occurs on the right-hand side of Eq. (83), ensures that the solution of the inhomogeneous equation also has this property.

Next we consider excitations caused by the two-body Coulomb interaction. For the single-particle Coulomb excitations, there will be a passive state which is involved in the interaction. For instance, at the first interaction line of diagram 5(d) and 5(e) a core orbital is excited due to an interaction with an electron in the open shell. The perturbed function which describes the mixing of excited states into the core orbital a by means of a *direct* interaction with an open-shell electron is

$$\rho_d^k(n_a l_a \to l_i\,; r) = \sum_{\text{exc } n_i} P_i(r)\frac{R^k(nln_i l_i,\, nln_a l_a)}{\epsilon_a - \epsilon_i} \ , \quad (84a)$$

where

$$R^k(abcd) = \int P_a(r)\frac{1}{r}Y^k(b,\,d;\,r)P_c(r)\,dr = \int P_a(r)\left(\int P_b(r')\frac{r_<^k}{r_>^{k+1}}P_d(r')\,dr'\right) \times P_c(r)\,dr \ .$$

In a manner which is similar to the derivation of Eq. (81), $\rho_d^k(n_a l_a \to l_i\,; r)$ may be shown to satisfy the equation[26]

$$(\epsilon_a - h_r^0)\rho_d^k(n_a l_a \to l_i\,; r) = \frac{1}{r}Y^k(nl,\,nl;\,r)P_a(r) - \sum_{\text{occ } n_i} P_i(r)R^k(nln_i l_i,\, nln_a l_a) \ . \quad (85)$$

Similarly, the excitation of a core electron by means of an *exchange* interaction with the open shell is described by the function

$$\rho_e^k(n_a l_a \to l_i\,; r) = \sum_{\text{exc } n_i} P_i(r)\frac{R^k(nln_i l_i,\, n_a l_a nl)}{\epsilon_a - \epsilon_i} \quad (84b)$$

which satisfies the equation

$$(\epsilon_a - h_r^0)\rho_e^k(n_a l_a \to l_i\,; r) = \frac{1}{r}Y^k(nl,\,n_a l_a\,; r)P_{nl}(r) - \sum_{\text{occ } n_i} P_i(r)R^k(nln_i l_i\,,\, n_a l_a nl) \ . \quad (86)$$

For *double* excitations we get in analogy with Eq. (77), the *"pair equation"*

$$[\epsilon_a+\epsilon_b-h^0(1)-h^0(2)]\eta(1,2)=\sum_{ij}|ij\rangle\langle A_{ab}^{ij}|QVP|A\rangle=\sum_{\text{exc }ij}|ij\rangle\langle ij|\frac{1}{r_{12}}|ab\rangle\ , \tag{87}$$

where the last summation shall be performed over all such combinations of ij such that $A_{ab}^{ij}\in Q$. This leads to the radial equation[26]

$$\begin{aligned}[\epsilon_a+\epsilon_b-h_r^0(1)-h_r^0(2)]\rho^k(n_al_a,n_bl_b\to l_il_j;r_1r_2)&=\sum_{\text{exc }n_in_j}P_i(r_1)P_j(r_2)R^k(n_il_in_jl_j,n_al_an_bl_b)\\&=\frac{r_<^k}{r_>^{k+1}}P_a(r_1)P_b(r_2)-\sum_{\text{occ }n_i}P_i(r_1)\frac{1}{r_2}Y^k(n_il_i,n_al_a;r_2)P_b(r_2)\\&\quad-\sum_{\text{occ }n_j}P_j(r_2)\frac{1}{r_1}Y^k(n_jl_j,n_bl_b;r_1)P_a(r_1)\\&\quad+\sum_{\text{occ }n_in_j}P_i(r_1)P_j(r_2)R^k(n_il_in_jl_j,n_al_an_bl_b)\ .\end{aligned} \tag{88}$$

To obtain this equation, we have used the identity

$$\sum_{\substack{\text{exc }n'\\ \text{exc }n''}}=\sum_{\substack{\text{all }n'\\ \text{all }n''}}-\sum_{\substack{\text{occ }n'\\ \text{all }n''}}-\sum_{\substack{\text{all }n'\\ \text{occ }n''}}+\sum_{\substack{\text{occ }n'\\ \text{occ }n''}}$$

which is the two-dimensional analog of Eq. (82). Here "excited" and "occupied" have similar meanings as before, the basic rule being that excitations $A_{ab}^{ij}\in Q$ shall be included. At least one of the excitations must therefore be "outside the model space," i.e., either from an open shell to an excited orbital or from the core to an open-shell or excited orbital. If there are several open shells, the other excitation can, in principle, occur between two such shells. Such excitations can also be treated by means of the one-particle equation, but it might often be convenient to include them in the pair excitations, if these are calculated. The explicit form of the pair function is

$$\rho^k(n_al_a,n_bl_b\to l_il_j;r_1r_2)=\sum_{\text{exc }n_in_j}P_i(r_1)P_j(r_2)\frac{R^k(n_il_in_jl_j,n_al_an_bl_b)}{\epsilon_a+\epsilon_b-\epsilon_i-\epsilon_j}\ . \tag{89}$$

C. Numerical treatment

The one-particle equations were solved numerically by means of subroutines taken from the Hartree-Fock program of Froese-Fischer.[28] This means that Numerov's method was used for the outward and inward integrations. Since the energy eigenvalues, which appear in the one-particle equations are known, the only undetermined quantity is the slope of the function at the origin. The slope is varied until the inward and outward integrations match.

The one-particle equations are similar in form to the hydrogen equation. So it is reasonable to assume that the accuracy with which we have solved the one-particle equation is comparable to the accuracy with which the corresponding subroutines solve the hydrogen equation. Froese-Fischer has checked her routines for hydrogen. The values of the mean radius, which she obtains, agree with the analytic solutions to five significant figures for $1s$ and $2s$ electrons and to four figures for $6s$ and $6p$ electrons.

The pair equation is considerably more difficult to solve. We use here the technique developed by Winter and co-workers.[23] The pair function is defined in a square-root grid, and a fourth-difference approximation is used for the derivatives. The two-particle equation is thus replaced by a matrix equation. In order to limit the size of the matrices involved, it is convenient to use two or three grids with a relatively small number of points and then to extrapolate the final results to a grid with zero interval. Winter checked this procedure for helium where the extensive calculation of Pekeris provides essentially an exact result. An accuracy of four significant figures was obtained in all cases. The pair functions used in the calculations presented here are normally defined on a grid having about 40 points in each direction, which means that a matrix equation of the order 1600×1600 has to be solved. This may usually be done very rapidly by relaxation methods; however, occasionally these methods do not converge properly, and it is necessary to solve the equations by Gaussian elimination. Because of the special form of the matrix, this can be done without the use of any external memory on our computer (IBM 360/65). Typical computing times for solving the pair function for 40×40 points by relaxation methods is 15 sec and by elimination 2 min, while the single-particle equation with a 200-point grid is solved in a fraction of a second.

D. Evaluation of radial factors

We are now in the position of evaluating the radial factors of the effective-operator diagrams, dis-

cussed in Sec. III. Let us first consider the second-order diagrams in Figs. 5(d) and 5(e). A single core orbital $(n_a l_a)$ is here excited into an excited or open-shell orbital $(n_i l_i)$ by means of the electrostatic interaction with the open shell (nl). According to Eq. (60a), the radial part of diagram 5(d) is

$$R_1^{(k_1)} = \sum_{\text{exc } n_i} \frac{\langle n_a l_a | r^{-3} | n_i l_i \rangle R^{k_1}(nl\, n_i l_i, nl\, n_a l_a)}{\epsilon_a - \epsilon_i} .$$

In order to evaluate this expression, we may draw the Slater integral and the energy denominator inside the first matrix element to obtain

$$R_1^{(k_1)} = \int dr\, P_a(r) r^{-3} \times \left(\sum_{\text{exc } n_i} \frac{R^{k_1}(nl n_i l_i, nl n_a l_a) P_i(r)}{\epsilon_a - \epsilon_i} \right) .$$

Using the perturbed function (84a), $R_1^{(k_1)}$ may thus be written

$$R_1^{(k_1)} = \langle n_a l_a | r^{-3} | \rho_d^{k_1}(n_a l_a \rightarrow l_i; r) \rangle\rangle . \quad (90)$$

Similarly, the radial factor for diagram 5(e) in Eq. (60b) becomes

$$R_2^{(k_1)} = \sum_{\text{exc } n_i} \frac{\langle n_a l_a | r^{-3} | n_i l_i \rangle R^{k_1}(nl\, n_i l_i, n_a l_a\, nl)}{\epsilon_a - \epsilon_i}$$

$$= \langle n_a l_a | r^{-3} | \rho_e^{k_1}(n_a l_a \rightarrow l_i, r) \rangle\rangle . \quad (91)$$

Alternatively, these diagrams can be evaluated by means of the hyperfine perturbed function

$$R_1^{(k_1)} = R^{k_1}(nl \rho_h(n_a l_a \rightarrow l_i; r), nl\, n_a l_a) , \quad (92)$$

$$R_2^{(k_1)} = R^{k_1}(nl \rho_h(n_a l_a \rightarrow l_i; r), n_a l_a\, nl) ,$$

where we have drawn the matrix element $\langle n_a l_a | r^{-3} | n_i l_i \rangle$ and energy denominator inside each Slater integral and made use of Eq. (80). Thus, we have a way of checking the numerical accuracy of the calculations.

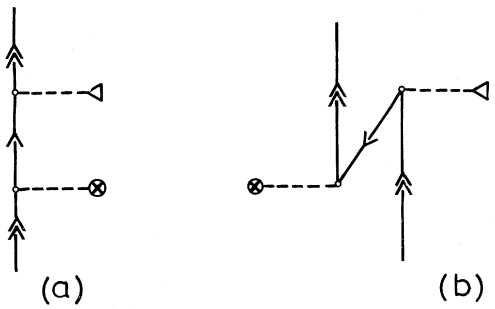

FIG. 14. Second-order potential diagrams.

As an example of the use of a pair function, we shall consider the evaluation of the diagram in Fig. 9(b). Using Eq. (89), the radial factor (70) can be expressed as

$$R_2^{(k_1 k_2)} = R^{k_1}(\rho_h(nl \rightarrow l_k; r_1) n_a l_a, \rho^{k_2}(nl, n_a l_a \rightarrow l_i l_j; r_1 r_2)) . \quad (93)$$

The pair function replaces here two orbitals in the Slater integral.

The examples given above should suffice to illustrate the use of perturbed functions to evaluate second- and third-order diagrams. The main advantage of this technique is that it is straightforward to calculate *all* effects to third order without explicit use of excited orbitals. If the perturbation theory converges so slowly that higher-order effects are important, this usually points to some inadequacy in the initial description of the atom. One might hope to include gross effects of this kind by modifying the approximate Hamiltonian or by extending the model space.[19]

There are two diagrams in second order we have not considered so far, namely, those involving a potential interaction (Fig. 14). These diagrams can, of course, be evaluated in the same way as the diagrams considered above, involving the two-body electrostatic interaction. However, we shall find it convenient to treat the potential interactions differently. Suppose we solve the radial equation corresponding to the potential interaction. Since the potential is spherically symmetric, it cannot mix different l, m_s, or m_l. The solution will therefore have the same spin-angular property as the orbital being excited (in this case an open-shell orbital). If we add the solution to the radial part of this orbital, we see that diagram (14a) is automatically included in the first-order diagram [Fig. 5(a)]. By relaxing the restriction that the solution shall be orthogonal to all core orbitals, which is due to the "orthogonality forcing terms" on the right-hand side of the inhomogeneous equations, we can also include the diagram (14b). In this way we have also included a large number of other diagrams, namely all where an open-shell line is "modified" by the po-

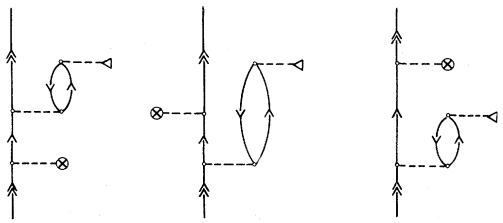

FIG. 15. Third-order diagrams for which an open-shell line is modified by the potential interaction.

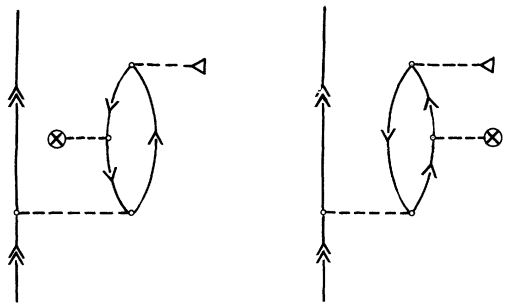

FIG. 16. Third-order diagrams for which a core and an excited orbital are modified by the potential interaction.

tential. For instance, the diagram in Fig. 5(d) will automatically include the diagrams in Fig. 15. In the same way we can eliminate other classes of diagrams involving potential interactions. By modifying the core orbitals as well as the one-particle perturbed functions, diagrams of the type shown in Fig. 16 are eliminated.

The potential modifications described above can, of course, be applied several times, corresponding to several potential interactions on a single line. In particular, the occupied orbitals can be modified until self-consistency is reached. Then a set of orbitals which satisfy some kind of Hartree-Fock condition is generated. We shall not consider the detailed structure of these corrections here but postpone that to a forthcoming paper.

The potential corrections considered above involve only nondiagonal elements, since the solution of the radial equation (83) is always orthogonal to the orbital being excited. Therefore, the diagonal elements require a special treatment. These lead to diagrams of "ladder" type, and they can easily be summed to all orders. Alternatively, we can eliminate these diagrams by means of a simple substitution. Let us replace the model Hamiltonian H_0 and the perturbation V by

$$H_0' = H_0 + \sum_i a_i^\dagger \langle i | v | i \rangle a_i \tag{94}$$

and

$$V' = V - \sum_i a_i^\dagger \langle i | v | i \rangle a_i ,$$

where v is the effective potential (Fig. 6). H_0' has the same eigenfunctions as H_0, but the single-electron energies are changed to

$$\epsilon_i' = \epsilon_i + \langle i | v | i \rangle . \tag{95}$$

In this way all diagonal elements of the potential perturbation are eliminated, and, instead, the energy denominators are modified. The same result is, of course, obtained by summing "ladder" diagrams to all orders.

Thus, we have seen that we can, in principle, eliminate the diagrams containing potential interactions. Instead of the modification procedure, described above, one could define the orbitals in such a way that the effective potential v is identically zero. For the occupied orbitals this is quite feasible, and corresponds to using some kind of HF orbitals. For the excited orbitals, on the other hand, this would imply that the inhomogeneous equations had to be solved iteratively. This can be accomplished with our programs, but we have found that the procedure described here yields essentially the same results in a much shorter time.

VI. RESULTS AND DISCUSSION

A. Analysis of numerical results

Because the pair equations can more easily be solved in a local potential, the present calculations were carried out using local potentials of the Hartree-Fock-Slater type.[29] As described in Sec. V, the difference between the local potential and the Hartree-Fock (HF) potential was then taken into account by successively solving the one-electron equation. This procedure leads to modified orbitals which are essentially the same as the HF functions, and it ensures that potential diagrams, which cancel exactly with Hartree-Fock orbitals, are quite small. In order to check this procedure, the calculation for the $2p$ state of Li was carried out using two different local potentials, the "optimized Hartree-Fock-Slater" (OHFS)[29] and the "Hartree-Slater" (HS) potentials.[30]

The first column of Table I shows the first-order values of $\langle r^{-3} \rangle$ for Li $2p$ obtained with these two local approximations and in restricted Hartree-Fock (HF). When the potential corrections described in Sec. V were done, the values given in column 2 were obtained. The influence of the different starting potentials is thus removed and the HF value is reproduced.

Since the potential diagrams shown in Fig. 5(b) and 5(c) are included in the modification procedure, the only second-order diagrams that must be calculated explicitly are those given in Fig. 5(d) and 5(e). The second-order values of $\langle r^{-3} \rangle$, which include these diagrams and the potential modification of the single-particle functions, are given in columns 3–5 of Table I for the orbital, spin-dipole, and quadrupole interactions, respectively. Again, the values of $\langle r^{-3} \rangle$ are essentially independent of the starting potential.

As we have said, there are 46 distinct third-order effective-operator diagrams without po-

TABLE I. Potential corrections for Li $2p$.

Potentials	First-order		Second-order		
	Uncorrected $\langle r^{-3}\rangle$	Potential corrected $\langle r^{-3}\rangle$	Potential corrected $\langle r^{-3}\rangle_l$	$\langle r^{-3}\rangle_{sd}$	$\langle r^{-3}\rangle_q$
OHFS	0.066 23	0.058 49	0.058 49	0.061 80	0.052 28
HS	0.072 39	0.058 46	0.058 46	0.061 76	0.052 25
HF	0.058 49	0.058 49	0.058 49	0.061 82	0.052 29

tential interaction. Of these diagrams, the 28 graphs, for which the hyperfine interaction occurs last, are shown in Figs. 7 and 8. The other 18 diagrams may be obtained by interchanging the order of the hyperfine and Coulomb interactions in these diagrams, so that the hyperfine interaction occurs in the middle. As discussed in Sec. III, the diagrams that occur in the perturbation expansion can be separated into core-polarization and correlation diagrams. The polarization diagrams can be evaluated using only single-particle functions, and they are implicitly included in the unrestricted Hartree-Fock (UHF). One inherent check of the accuracy of our calculation is the extent to which our third-order core-polarization values agree with UHF calculations. As we shall see, the agreement is quite good. The correlation diagrams contain two or more excited state lines at a time, and they are not properly included in any single-particle theory, no matter how deviously it is constructed.

The most important third-order core-polarization diagrams were found to be 7(a) and 7(b). For the excited p states of Li, 7(a) only contributes to the quadrupole term while 7(b) also contributes to the spin-dipole interaction. As is easily seen, these diagrams are obtained from the second-order polarization graphs, shown in Fig. 5, by letting the excited electron-hole pair interact in a direct way. A summary of the polarization effects is given in Table II. The remaining third-order diagrams, which require the use of one or two pair functions, provide the leading correlation effects. The most important diagram of this kind is shown in Fig. 8(a). This diagram can be regarded as a modification of the correlation energy of an open-shell electron and a core electron by the hyperfine interaction. This single very important graph, which contributes to all three hyperfine parameters, is of the same order of magnitude as the second-order polarization contribution and the entire third-order correlation effect. Diagram 8(b) is an exchange version of 8(a). For each choice of the angular momenta of the excited states, this diagram gives a contribution which is nearly as large as that of the corresponding direct diagram. The different contributions tend to cancel, however, and the total effect of this diagram is quite small. Exchange diagrams often have this property.

The graph 8(m), which only contributes to the quadrupole interaction, was also found to be important. It may also be regarded as a modification of the correlation energy of an open-shell core-electron pair. In this diagram, though, it is the

TABLE II. Core polarization effects for Li $2p$.

Diagrams	Contribution to $\langle r^{-3}\rangle_{sd}$	Contribution to $\langle r^{-3}\rangle_q$
Second order:		
5(d)	•••	−0.009 52
5(e)	0.003 31	0.003 31
Third order:		
7(a)	•••	−0.001 55
7(b)	0.000 64	0.000 64
Other diagrams	0.000 07	0.000 27
Total	0.004 02	−0.006 85

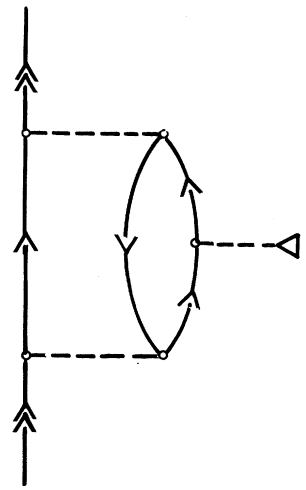

FIG. 17. Third-order diagram having two excited lines throughout. This diagram is evaluated using two pair functions.

core-electron line which is modified by the hyperfine interaction. The largest diagram involving correlation between the two 1s electrons in the core is 8(c). As a result of the Pauli principle, one half of this diagram is cancelled by 8(d).

The correlation graphs discussed so far can be evaluated using one pair function and one single-particle hyperfine function. Diagrams, which have two excited lines throughout, were evaluated using two pair functions. These diagrams were usually found to be very small. For the $2p$ state of Li, the largest diagram of this kind is shown in Fig. 17.

A summary of the correlation contributions for the $2p$ state of Li is given in Table III and a summary of the complete calculation to third order is given in Table IV and Fig. 18. The third-order core-polarization diagrams are considerably smaller than the corresponding second-order diagrams. This indicates a satisfactory convergence of the core-polarization contributions. In principle these polarization effects are included exactly in the unrestricted Hartree-Fock (UHF), and the good agreement between our third-order polarization value and the UHF calculation of Lunell[37] is also encouraging. Correlation effects, however, arise for the first time at third order, so it is not possible to tell from our calculation itself how rapidly the correlation effects converge. Higher-order correlation diagrams can be evaluated by solving the one- and two-electron equation successively. Until this is done, the correlation contributions remain tentative, and we can only point to the good agreement between our results and experiment.

Thus far, we have only discussed the $2p$ state of Li. The nature of the various contributions to the hyperfine structure of the $3p$ and $4p$ states of Li is quite similar. There is a clear tendency, however, for the relative contribution of correlation to decrease with increasing principal quantum number. This is to be expected because the main correlation contributions are due to the interaction between the 1s core and the open-shell p electron.

TABLE III. Summary of the correlation contributions for the Li $2p$ state.

Diagrams	Contribution to $\langle r^{-3}\rangle_l$	$\langle r^{-3}\rangle_{sd}$	$\langle r^{-3}\rangle_q$
8(a)	0.004 41	0.004 41	0.004 41
8(b)	−0.000 18	−0.000 18	−0.000 18
8(m)	•••	•••	0.001 65
8(c) + 8(d)	−0.000 29	−0.000 29	−0.000 29
17	−0.000 05	•••	0.000 42
Other diagrams	0.000 43	0.000 18	−0.000 98
Total	0.004 32	0.004 12	0.005 03

TABLE IV. Summary of the present calculations (OHFS) for the Li $2p$ state.

Calculations	$\langle r^{-3}\rangle_l$	$\langle r^{-3}\rangle_{sd}$	$\langle r^{-3}\rangle_q$
First order	0.066 23	0.066 23	0.066 23
Potential correction	−0.007 74	−0.007 74	−0.007 74
First order after potential correction	0.058 49	0.058 49	0.058 49
Second-order polarization	•••	0.003 31	−0.006 21
Third-order polarization	•••	0.000 71	−0.000 64
Third order including polarization	0.058 49	0.062 51	0.051 64
UHF[a]	0.058 62	0.063 21	0.052 11
Correlation	0.004 32	0.004 12	0.005 03
Total third order	0.062 81	0.066 63	0.056 67

[a] Reference 47.

The final results for the $3p$ and $4p$ states of Li are given in Table V.

Our results for the $3p$ state of Na are summarized in Table VI and in Fig. 19. The local OHFS potential was used and, as for Li, the potential modifications were applied. The first-order corrected value of $\langle r^{-3}\rangle$, 0.1676, agrees well with the HF result. The third row of Table VI shows the second-order contribution of core polarization to the different effective $\langle r^{-3}\rangle$ values. The dom-

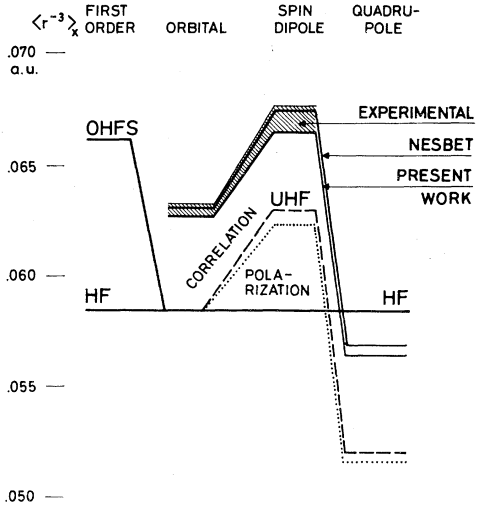

FIG. 18. Radial parameters for the effective magnetic dipole and electric quadrupole operators for Li $2p$. Dotted line represents the polarization result in third-order perturbation and the dashed line the unrestricted HF result, which is equivalent to polarization to infinite order. Results of Nesbet and of the present work represents full many-body calculations (to at least third order in perturbation). Shaded region represents the experimental values (with their uncertainties) of the parameters of the dipole operator.

TABLE V. Comparison between theory and experiments for Li $2p$, $3p$, $4p$.

	$\langle r^{-3}\rangle_l$	$\langle r^{-3}\rangle_{sd}$	$\langle r^{-3}\rangle_q$
Present calculation:		Li $2p$	
with OHFS potential	0.062 81	0.066 63	0.056 67
with HS potential	0.062 88	0.066 71	0.056 75
UHF[a]	0.058 62	0.063 21	0.052 11
Nesbet[b]	0.063 21	0.067 62	0.057 06
Das *et al.*[c]	0.062 82	0.068 59	(0.048 50)
Hameed & Foley[d]	•••	•••	0.058 00
Experiment[e]	0.063 09(31)	0.067 23(58)	•••
		Li $3p$	
First-order potential corrected	0.017 64	0.017 64	0.017 64
Second-order polarization	•••	0.001 10	−0.001 64
Third-order polarization	•••	0.000 23	−0.000 16
Third-order without correlation	0.017 64	0.018 97	0.015 84
Correlation	0.001 04	0.000 97	0.001 24
Total third-order value	0.018 68	0.019 94	0.017 08
UHF[f]	0.017 65	0.018 91	0.015 71
Experiment	0.019 10[g,h]		
	0.018 66[f]	0.020 53[f]	
		Li $4p$	
First-order potential corrected	0.007 452	0.007 452	0.007 452
Second-order polarization	•••	0.000 478	−0.000 653
Third-order polarization	•••	0.000 100	−0.000 063
Third-order without correlation	0.007 452	0.008 030	0.006 736
Correlation	0.000 406	0.000 378	0.000 494
Total third-order value	0.007 858	0.008 408	0.007 230
UHF[f]	0.007 443	0.008 018	0.006 696
Experiment	0.008 06[h]		
	0.007 95[f]	0.008 75[f]	

[a]Reference 47.
[b]Reference 4.
[c]Reference 25.
[d]Reference 6.
[e]Reference 34.
[f]Reference 37.
[g]Reference 35.
[h]Reference 36.

inant part of this effect is due to the polarization of the $2p$ shell. In the fourth row of Table VI the third-order polarization contribution is given, and as in the Li case, the main contribution is due to the diagrams shown in Fig. 7(a) and 7(b). The largest effect is the scattering of a $2p$ state to another p state thus giving rise to a radial distortion of the core. Turning to the correlation diagrams, it is found that diagrams of importance in the Li case also contribute significantly for Na. However, because of the presence of p electrons in the core, diagrams 8(i)–8(l), which do not contribute for Li, have an important effect. These diagrams describe correlation effects between core electrons, the main contribution being due to $2p$ intershell correlation. A summary of the correlation contributions is given in Table VII, and the total third-order values for the $3p$ state of Na

TABLE VI. Summary of the present calculations for Na $3p$.

Calculations	$\langle r^{-3}\rangle_l$	$\langle r^{-3}\rangle_{sd}$	$\langle r^{-3}\rangle_q$
First order (OHFS)	0.2365	0.2365	0.2365
Potential corrections	−0.0689	−0.0689	−0.0689
Second-order polarization	0.0343	0.0390	0.0630
Third-order polarization	0.0112	0.0130	0.0225
Third-order without correlation	0.2131	0.2196	0.2531
Correlation	0.0202	0.0204	0.0155
Total third-order value	0.2333	0.2400	0.2686

in row seven of Table VI.

Our procedure of calculating the second- and third-order diagrams is entirely automatic. The Li $2p$ calculation took about 17 min on the IBM 360/65 computer, and a calculation of the hyperfine constants for another atomic state requires essentially only changing the input cards of the one-particle and two-particle programs and the program for evaluating the Feynman diagrams.

B. Comparison with other *ab initio* calculations

Our total third-order values of the effective $\langle r^{-3}\rangle$ coefficients for the $2p$ state of Li are presented in the first two rows of Table V. As mentioned, two local potentials, OHFS and HS, have been used, but the final result is almost independent of the starting potential. There are higher-order potential corrections involving two excited states at a time that are not included within our modification procedure, so this small discrepancy is not difficult to understand.

Several extensive *ab initio* calculations have been carried out for the $2p$ state of Li. Nesbet,[4] using a variational approach, obtained the values given in the fourth row of Table V. There is good agreement between his and our results. For both of the potentials we used, our values are in agreement with his to about 1% in all cases. Since the methods are so different, this close agreement is encouraging. Das and coworkers,[25] using third-order perturbation theory, obtained the values given in row five. For the orbital and spin-dipole cases, there is a general agreement between the values which they provide for their Feynman diagrams and ours. So the agreement of the total result which appears between our calculations for these cases is not accidental. For the quadrupole case, however, there are numerous discrepancies between their diagrams and ours.

The quadrupole interaction has also been calculated by Hameed and Foley[6] and their value is given in row six. It deviates from Nesbet's and our results by about 2%. Most of this discrepancy is for the correlation contribution, and it is probably due to the limited number of configurations which Hameed and Foley used to construct the first-order wave function. For the $3p$ and $4p$ states of Li and the $3p$ state of Na our final results are given in Tables V and VI and represent the first accurate many-body calculations for these states. The UHF values of Lunell[37] for the p series of Li are included in our Table V, and these values should be compared with our "third-order values without correlation." As we have said, the agreement is very good, indicating that the higher-order polarization terms are quite small.

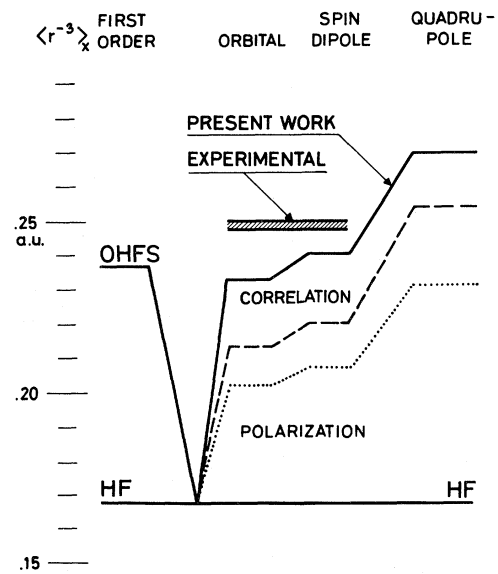

FIG. 19. Radial parameters for the effective magnetic dipole and electric quadrupole operators for Na $3p$. Dotted and dashed lines represent the polarization results in second- and third-order perturbation, respectively. Full line represents a complete third-order calculation and the shaded region the experimental average of the orbital and the spin-dipole parameters.

C. Comparison with experiments

An early experimental determination of the magnetic interaction constant $a_{1/2}$ for ^{6}Li and ^{7}Li in the $2p$ state was done by Ritter,[31] using the optical double resonance (ODR) method. Brog *et al.*[32] studied the fine-structure crossings in $2p$ using level crossing (LC) spectroscopy. Combining the information from both measurements, Lyons and Das[33] deduced effective $\langle r^{-3}\rangle$ values for the operators s, l, $(sC^2)^1$ occurring in the magnetic dipole case. Recently, using the ODR method,

TABLE VII. Correlation for Na $3p$.

Diagrams	$\langle r^{-3}\rangle_l$	Contribution to $\langle r^{-3}\rangle_{sd}$	$\langle r^{-3}\rangle_q$
8(a)	0.0429	0.0429	0.0429
8(b)	−0.0081	−0.0081	−0.0081
8(k)	0.0326	0.0326	0.0326
8(i)	−0.0195	−0.0195	−0.0195
8(j)	0.0058	0.0058	0.0058
8(l)	−0.0089	−0.0089	−0.0089
8(c)+8(d)	−0.0128	−0.0128	−0.0128
8(g)	−0.0098	−0.0102	−0.0102
8(m)	−0.0003		−0.0076
Others	−0.0017	−0.0014	0.0013
Total	0.0202	0.0204	0.0155

Orth[34] has studied the energy separation between Zeeman levels of the $2\,^2P_{1/2}$ and $2\,^2P_{3/2}$ states by scanning a magnetic field, with the frequency being kept to 10 GHz. From his data, alone, the same effective $\langle r^{-3}\rangle$ values could be obtained. The results are presented in Table V and Fig. 18. As can be seen the agreement between theory and experiments is quite good.

For the $3p$ state in ^{7}Li, level-crossing experiments have been performed by Budick *et al.*[35] and Isler *et al.*[36] However, in their analysis of the experimental data, a two-parameter description is used. This is also the case for the $4p$ state of ^{7}Li measured by Isler *et al.*[36] Lunell[37] has reanalyzed their data using the following assumptions: for the $2p$, $3p$, and $4p$ state the ratio $\langle r^{-3}\rangle_{sd}/\langle r^{-3}\rangle_l$ is supposed to be constant (in an unrestricted Hartree-Fock calculation this is essentially true) and for the $4p$ state a $1/n^3$ scaling of the parameter is further assumed. As can be seen from Table V, the agreement between his reanalyzed values and our theoretical ones for $3p$ is within 3% for the effective integrals and for $4p$ within 4%. The latter deviation might be explained by the rough $1/n^3$ scaling performed for the $4p$ level.

For Na $3p$ there are several experimental hyperfine measurements. Ackermann[38] and Baumann[39] have used ODR to measure the interaction constants $a_{3/2}$ and $b_{3/2}$. Schönberner and Zimmermann,[40] Baumann,[41] and Mashinski[42] have used LC, and Copley *et al.*[43] and Figger and Walther[44] used delayed level crossing (DLC) to measure the same constants. For the $a_{3/2}$ value the measurement of Schönberner and the one performed by Figger seem to be more reliable than the experiment of Mashinski, even though Mashinski gives a much smaller estimate of his error. The $a_{1/2}$ value for Na $3p$ has been determined by Rabi *et al.*[45] and Hartmann.[46]

No measurement of the off-diagonal hyperfine constant has been reported for the $3p$ state in Na, and therefore it is not possible to obtain experimental values for all three parameters of the effective dipole operator. Furthermore, we have in the present work not calculated the effective contact interaction and we can therefore not compare with the a factors directly. However, one can easily show the following relation:

$$a_{1/2} + a_{3/2} = K \times g_I (2\langle r^{-3}\rangle_l + \tfrac{6}{5}\langle r^{-3}\rangle_{sd}) \ .$$

If a is measured in MHz, $\langle r^{-3}\rangle$ in atomic units, and g_I in nuclear magnetons, then K has the value 95.412 85. Using this relation we can define an "average" of the orbital and spin-dipole parameters

$$\langle r^{-3}\rangle_{\rm ave} = \tfrac{5}{8}\langle r^{-3}\rangle_l + \tfrac{3}{8}\langle r^{-3}\rangle_{sd} = \tfrac{5}{16}(a_{1/2} + a_{3/2})/Kg_I \ .$$

From the experimental values of Hartmann[46] and Figger *et al.*[44] we obtain

$$\langle r^{-3}\rangle_{\rm ave}^{\rm expt} = 0.2502(11) \ .$$

By subtracting from this an estimate of the relativistic effects,[48] we obtain a "nonrelativistic" experimental value

$$\langle r^{-3}\rangle_{\rm ave}^{\rm nonrel} = 0.2485(11) \ .$$

The corresponding theoretical value obtained from our third-order results in Table VI is

$$\langle r^{-3}\rangle_{\rm ave}^{\rm nonrel} = 0.2358 \ .$$

A measurement of the off-diagonal hyperfine parameter for this state would be very helpful, since it would allow a more detailed comparison between the theoretical and experimental results.

D. Evaluation of quadrupole moments

The experimental quadrupole interaction constants for the states considered here are given in Table VIII together with the corresponding quadrupole moments obtained by means of our *ab initio* effective $\langle r^{-3}\rangle$ values. As a comparison, we have in the same table given also the quadrupole moments evaluated in the standard semiempirical procedure, using the experimental magnetic hfs constant and the quadrupole shielding factor given by Sternheimer.[22]

TABLE VIII. Calculated quadrupole moments.

Atom	State	$\langle r^{-3}\rangle_{\rm ave}^{\rm mag}$	R[a]	$\langle r^{-3}\rangle_q$	b_{ex} (Mhz)	Q[b] (mB)	$Q_{\rm ST}$[c] (mB)
^{7}Li	$2p$	0.064 24	0.117	0.056 67	−0.221(29)[d]	−41(5)	−41(5)
^{23}Na	$3p$	0.2358	−0.181	0.2686	3.04(19)[e]	120(8)	116(8)

[a] Factor given by Sternheimer, see Ref. 22.
[b] Quadrupole moment evaluated using our *ab initio* value $\langle r^{-3}\rangle_q$.
[c] Quadrupole moment obtained from the average $\langle r^{-3}\rangle$ value, calculated from experimental hfs, and using Sternheimer's correction factors.
[d] Reference 34.
[e] Reference 44.

Sternheimer's correction factors are obtained by solving a one-particle inhomogeneous differential equation of the type discussed in Sec. V, and they correspond to the second-order core-polarization diagrams [Fig. 5(d) and 5(e)]. Correlation effects are not included in these factors, and, furthermore, only the perturbation of the quadrupole interaction is taken into account. The magnetic dipole interaction is also perturbed in a similar way and this should be considered when the $\langle r^{-3} \rangle$ value for the quadrupole interaction is estimated in a semiempirical way.

It follows from what is said above that when the $\langle r^{-3} \rangle$ value for the quadrupole interaction is estimated from the magnetic hfs, the conventional Sternheimer factors can be expected to yield accurate results if the following two conditions are fulfilled: (i) the effect of core polarization on the magnetic hyperfine interaction is small and (ii) electron correlation has the same effect on the magnetic dipole and electric quadrupole interactions. From our results discussed above, we see that these conditions are well fulfilled for the $3p$ state in Na but less so for the p states in Li. The apparent agreement between the quadrupole moments for Li obtained with Sternheimer's method and from our calculation is accidental, because the effect of polarization upon the magnetic interaction essentially cancels the effect of correlation. One can expect that the conditions for heavier alkalis should be similar to that for Na, or, in other words, that the quadrupole moments evaluated in the standard way from hfs data for the p series should be fairly accurate. Preliminary calculations on the d states,[49] however, indicate that it is necessary to include the polarization effect on the magnetic interaction, if the semiempirical procedure shall be used to evaluate the quadrupole moment.

[1]K. A. Brueckner, Phys. Rev. 100, 36 (1955).
[2]J. Goldstone, Proc. R. Soc. Lond. A 239, 267 (1957).
[3]H. P. Kelly, Phys. Rev. 131, 684 (1963); 144, 39 (1966); Adv. Chem. Phys. 14, 129 (1969).
[4]R. K. Nesbet, Phys. Rev. 109, 1632 (1958); Phys. Rev. A 2, 661 (1970); Adv. Chem. Phys. 14, 1 (1969).
[5]A. W. Weiss, Phys. Rev. 122, 1826 (1961); 162, 71 (1967).
[6]S. Hameed and H. M. Foley, Phys. Rev. A 6, 1399 (1972).
[7]J. S. M. Harvey, Proc. R. Soc. Lond. A 285, 581 (1965).
[8]See, for instance, I. Lindgren and A. Rosén, Case Stud. At. Phys. 4, 93 (1974), where most hyperfine data presently available have been reanalyzed using the effective-operator technique.
[9]R. J. Eden and N. C. Francis, Phys. Rev. 97, 1366 (1955).
[10]H. Feshbach, Ann. Phys. (N.Y.) 5, 357 (1958); 19, 287 (1962).
[11]C. Bloch and J. Horowitz, Nucl. Phys. 8, 91 (1958).
[12]B. H. Brandow, Rev. Mod. Phys. 39, 771 (1967).
[13]B. R. Judd, Proc. Phys. Soc. Lond. A 289, 97 (1965); *Second Quantization and Atomic Spectroscopy* (Johns Hopkins, Baltimore, 1967).
[14]K. Rajnak and B. G. Wybourne, Phys. Rev. 132, 280 (1963).
[15]R. E. Trees, Phys. Rev. 83, 756 (1951).
[16]G. Racah, Phys. Rev. 85, 381 (1952).
[17]C. Bloch, Nucl. Phys. 6, 91 (1958).
[18]P. G. H. Sandars, Adv. Chem. Phys. 14, 365 (1969).
[19]I. Lindgren, J. Phys. (B) 7, 2441 (1975).
[20]M. B. Johnson and M. Baranger, Ann. Phys. (N.Y.) 62, 172 (1971); T. T. S. Kuo, S. Y. Lee, and K. F. Ratcliff, Nucl. Phys. A 176, 65 (1971); B. R. Barrett and M. W. Kirson, Prog. Nucl. Phys. 6, 219 (1973).
[21]A. P. Yutsis (Jucys), I. B. Levinson, and V. V. Vanagas, *Mathematical Apparatus of the Theory of Angular Momentum* (Israel Program for Scientific Translations, Jerusalem, 1962).
[22]R. M. Sternheimer, Phys. Rev. A 3, 837 (1971).
[23]V. McKoy and N. M. Winter, J. Chem. Phys. 48, 5514 (1968); J. I. Musher and J. M. Schulman, Phys. Rev. 173, 93 (1968).
[24]J. C. Morrison and K. Rajnak, Phys. Rev. A 4, 536 (1971).
[25]J. D. Lyons, R. T. Pu, and T. P. Das, Phys. Rev. 178, 103 (1969).
[26]J. C. Morrison, Phys. Rev. A 6, 643 (1972); J. Phys. B 6, 2205 (1973).
[27]J. M. Schulman and W. S. Lee, Phys. Rev. A 5, 13 (1972).
[28]C. Froese-Fischer, Can. J. Phys. 41, 1895 (1963).
[29]I. Lindgren, Phys. Lett. 19, 382 (1965); Ark. Fys. 31, 59 (1966).
[30]I. Lindgren, Int. J. Quantum Chem. 5, 411 (1971); I. Lindgren and K. Schwarz, Phys. Rev. A 5, 542 (1972).
[31]G. J. Ritter, Can. J. Phys. 43, 770 (1965).
[32]K. C. Brog, T. G. Eck, and H. Wieder, Phys. Rev. 153, 91 (1967).
[33]J. D. Lyons and T. P. Das, Phys. Rev. A 2, 2250 (1970).
[34]H. Orth, Diplom-Arbeit 1970 (private communication).
[35]B. Budick, H. Bucka, R. J. Goschen, A. Landman, and R. Novick, Phys. Rev. 147, 1 (1966).
[36]R. C. Isler, S. Marcus, and R. Novick, Phys. Rev. 187, 76 (1969).
[37]S. Lunell, Phys. Rev. A 7, 1229 (1973).
[38]H. Ackermann, Z. Phys. 194, 253 (1966).
[39]M. Baumann, W. Hartmann, H. Krüger, and A. Oed, Z. Phys. 194, 270 (1966).
[40]D. Schönberner and D. Zimmermann, Z. Phys. 216,

172 (1968).
[41]M. Baumann, Z. Naturforsch. A 21, 1049 (1969).
[42]A. L. Mashinski, Opt. Spektrosk. 28, 3 (1970).
[43]G. Copley, B. P. Kibble, and G. W. Series, J. Phys. B 1, 724 (1968).
[44]H. Figger and H. Walther, Z. Phys. 267, 1 (1974).
[45]M. L. Perl, I. I. Rabi, and B. Senitzky, Phys. Rev. 98, 611 (1955).
[46]W. Hartmann, Z. Phys. 240, 323 (1970).
[47]S. Larsson, Phys. Rev. A 2, 1248 (1970).
[48]A. Rosén and I. Lindgren, Phys. Scr. 6, 109 (1972).
[49]S. Garpman, I. Lindgren, J. Lindgren, and J. Morrison (unpublished).